RMetS
Royal Meteorological Society

Global energy budgets and 'Trenberth diagrams' for the climates of terrestrial and gas giant planets

P. L. Read,[a]* J. Barstow,[a] B. Charnay,[b] S. Chelvaniththilan,[a] P. G. J. Irwin,[a] S. Knight,[c] S. Lebonnois,[b] S. R. Lewis,[d] J. Mendonça[a,e] and L. Montabone[b,f]

[a]*Department of Physics, Clarendon Laboratory, University of Oxford, UK*
[b]*Laboratoire de Météorologie Dynamique, Université Pierre et Marie Curie, Paris, France*
[c]*Royal Meteorological Society, Reading, UK*
[d]*Department of Physical Sciences, The Open University, Milton Keynes, UK*
[e]*Center for Space and Habitability, University of Bern, Switzerland*
[f]*Space Science Institute, Boulder, CO, USA*

*Correspondence to: P. L. Read, Atmospheric, Oceanic & Planetary Physics, Clarendon Laboratory, Parks Road, Oxford, OX1 3PU, UK. E-mail: p.read1@physics.ox.ac.uk

The climate on Earth is generally determined by the amount and distribution of incoming solar radiation, which must be balanced in equilibrium by the emission of thermal radiation from the surface and atmosphere. The precise routes by which incoming energy is transferred from the surface and within the atmosphere and back out to space, however, are important features that characterize the current climate. This has been analyzed in the past by several groups over the years, based on combinations of numerical model simulations and direct observations of the Earth's climate system. The results are often presented in schematic form to show the main routes for the transfer of energy into, out of and within the climate system. Although relatively simple in concept, such diagrams convey a great deal of information about the climate system in a compact form. Such an approach has not so far been widely adopted in any systematic way for other planets of the Solar System, let alone beyond, although quite detailed climate models of several planets are now available, constrained by many new observations and measurements. Here we present an analysis of the global transfers of energy within the climate systems of a range of planets within the Solar System, including Mars, Titan, Venus and Jupiter, as modelled by relatively comprehensive radiative transfer and (in some cases) numerical circulation models. These results are presented in schematic form for comparison with the classical global energy budget analyses for the Earth, highlighting important similarities and differences. We also take the first steps towards extending this approach to other Solar System and extrasolar planets, including Mars, Venus, Titan, Jupiter and the 'hot Jupiter' exoplanet HD 189733b, presenting a synthesis of both previously published and new calculations for all of these planets.

Key Words: energy budget; radiative heat flux; sensible heat flux; climate equilibrium; planetary atmospheres

Received 26 November 2014; Revised 17 October 2015; Accepted 3 November 2015; Published online in Wiley Online Library 3 February 2016

1. Introduction

The climate of a planet like the Earth is largely determined by the flow of energy into and out of the top of the atmosphere and at the surface (e.g. Trenberth *et al.*, 2009; Stephens *et al.*, 2012; IPCC, 2013; Wild *et al.*, 2013). Solar radiation illuminates the atmosphere and surface, mainly in the visible, near-infrared and ultraviolet parts of the spectrum, which is ultimately balanced by longer wavelength radiative exchanges from the surface and atmosphere in an equilibrium climate. Note that we restrict attention here to atmospheres below their respective thermospheres and ionospheres, where the physics and chemistry differ markedly from lower altitudes, e.g. at altitudes below around 85 km for the Earth, and where energy exchanges contribute very little to the global energy budget. The vertical and geographical variations in these energy flows lead to local imbalances that can

drive circulation and motions in the atmosphere and/or oceans associated with sensible heat fluxes, the details of which may depend strongly on other features of the planet – its size, rotation rate, obliquity, etc. The presence of condensible species with associated latent heat of condensation or fusion can complicate the energy budget of the planet further, enabling another channel for energy flow associated with the transfer of condensible mass within the diabatically driven circulations. Even small (but systematic) imbalances in the global energy budget may lead to slow but perceptible changes in the climate as it adjusts towards equilibrium, which are, of course, one of the main preoccupations of the recent IPCC assessment reports (e.g. IPCC, 2013).

Attempts to quantify the global energy flow through the Earth's climate system have been carried out for more than 100 years, beginning with the early calculations by Abbot and Fowle (1908) and Dines (1917). However, such early assessments were fraught with uncertainties through a lack of global measurements of even such basic quantities as the albedo (or ratio of outgoing, reflected and scattered solar energy to the incident flux), for which early estimates, for example, ranged from 29–80% (Vonder Haar and Suomi, 1971). The most recent and accurate assessments of the detailed energy balance of the Earth's climate system rely heavily on combinations of highly sophisticated and carefully calibrated radiometer instruments in Earth orbit, together with complex numerical models that seek to compute the detailed exchanges of radiative and mechanical energy within the atmosphere and oceans. Such instruments and models provide global coverage of the whole planet over a wide range of phase angles, allowing a detailed and accurate assessment of both global and regional exchanges of radiation at the top of the atmosphere.

The results of such analyses are traditionally averaged across the globe in a schematic form that is often referred to as a 'Trenberth diagram' (e.g. Kiehl and Trenberth, 1997; Trenberth *et al.*, 2009; Stephens *et al.*, 2012), in which upward and downward energy fluxes at the surface, top of the atmosphere and (sometimes) intermediate levels are portrayed in graphical form. Such diagrams convey a lot of information very compactly and can be useful for understanding the way in which the atmosphere comes into energetic balance with the surface and solar insolation.

Given the widespread use of such diagrams in the research and review literature and in elementary textbooks on the Earth's climate system, it is somewhat surprising that this approach has not been taken up with more enthusiasm in the context of other planetary atmospheres. Although isolated examples of similar diagrams to those published for the Earth can be found for planets such as Venus (e.g. Taylor, 2010; Titov *et al.*, 2013) and Mars (e.g. Read and Lewis, 2004; Taylor, 2010), these are typically incomplete and of doubtful accuracy in some cases, often relying on relatively crude estimates of key parameters. A recent exception to this can be found in the work of Schubert and Mitchell (2013), in which a more systematic approach has been taken, at least for Venus, Mars and Titan, with the intention of developing an assessment of the rates of entropy production and thermodynamic efficiency, treating those atmospheres (and that of the Earth itself) as classical heat engines (Peixoto and Oort, 1992). Such an approach offers the potential for some interesting insights into how atmospheres process energy and entropy to achieve a balance between energy production and dissipation (e.g. Ozawa *et al.*, 2003; Lucarini, 2009; Lucarini and Ragone, 2011). To realize this potential fully, however, generally requires computing not only the boundary fluxes of radiative, sensible and latent energy but also the internal energy conversions, as represented, for example, in the classical Lorenz energy cycle (Lorenz, 1955, 1967).

The latter generally requires a more detailed array of measurements or model simulations than is yet widely available for planets other than the Earth, although this situation is beginning to change as more data from spacecraft become available. However, the data needed to apply the 'Trenberth diagram' approach may now be compiled from combinations of existing measurements and model simulations for a number of planets and this article seeks to address this approach in an attempt to produce a reasonably robust set of comparative 'Trenberth diagrams' for a series of planets that are representative of those found in our Solar System. Accordingly, in the following sections we present and review recent analyses for the Earth (section 2) and compare these with new analyses compiled here for Mars, Venus, Titan and Jupiter's 'weather layer' (in sections 3–6). In addition, new classes of planets are now being discovered in increasing numbers around other stars (Schneider *et al.*, 2011). One of the most well studied of these classes is the so-called 'hot Jupiter' planet, comprising a gas giant of comparable size to Jupiter but located very close to its parent star, such that its rotation is almost certainly locked to its orbital period and its day side is extremely intensively irradiated. Observations and models are beginning to provide some interesting constraints on the flow of energy within and through such planets and so we present here in section 7 a first attempt to compile a 'Trenberth-style diagram' for such a planet. These analyses are then compared and discussed in the final section 8.

2. Earth

2.1. Data sources

Unsurprisingly, the Earth's energy budget has been quantified in the most detail and to relatively high precision. Even so, a number of significant uncertainties persist, partly because some fluxes (such as those of sensible and latent heat) are very difficult to measure accurately in remote regions, but also because of intrinsic calibration errors for some of the top of atmosphere (TOA) radiative measurements from satellites. The incoming solar flux (or solar irradiance) is known to the highest accuracy at $340.2 \pm 0.1\,\mathrm{W\,m^{-2}}$ (Kopp and Lean, 2011) and varies the least of all the other fluxes. For the other fluxes, estimates vary as to their likely uncertainty, from around $1\,\mathrm{W\,m^{-2}}$ for some to around $10\,\mathrm{W\,m^{-2}}$ for the least well-characterized quantities, associated e.g. with latent heat and evapotranspiration and certain effects of clouds (Trenberth *et al.*, 2009; Stephens *et al.*, 2012; Wild *et al.*, 2013), or even greater for some surface fluxes. The overall results, together with assessments of changes in ocean heat content over a decade of observations (Hansen *et al.*, 2011; Loeb *et al.*, 2012), indicate a net imbalance between incoming and outgoing energy fluxes of around $0.6 \pm 0.4\,\mathrm{W\,m^{-2}}$, thought to represent the overall warming trend in the current climate (IPCC, 2013).

Figure 1 summarizes the recent set of estimates obtained from combinations of remote sensing and *in situ* measurements, together with well-validated numerical model simulations (e.g. Kim and Ramanathan, 2012; Trenberth and Fasullo, 2012; Stephens *et al.*, 2012; Wild *et al.*, 2013) and compiled for the 5th Assessment Report of the Intergovernmental Panel on Climate Change (IPCC, 2013). These represent some of the most comprehensive studies to date that include strenuous efforts to trace the uncertainties in all of the main fluxes. They update the earlier work of Trenberth *et al.* (2009), which used a similar mix of data sources and reanalysis data instead of free-standing model simulations. Figure 1 thus represents the current state of the art in deriving such an energy budget for an entire planet. Anticipating how this approach will be adapted in the following sections for other planets, we present the flux data in Figure 1 directly in $\mathrm{W\,m^{-2}}$ *and* with each flux normalized by the incoming solar irradiance (which is given 100 dimensionless *irradiance percentage units* or IPU). This helps to see how the energy in the system is partitioned into various upward and downward channels and also helps to emphasize features such as the greenhouse warming of the surface.

2.2. Global energy budget

Thus, the picture for the Earth is seen to be quite a complicated one, in which the atmosphere plays a major role in modifying the

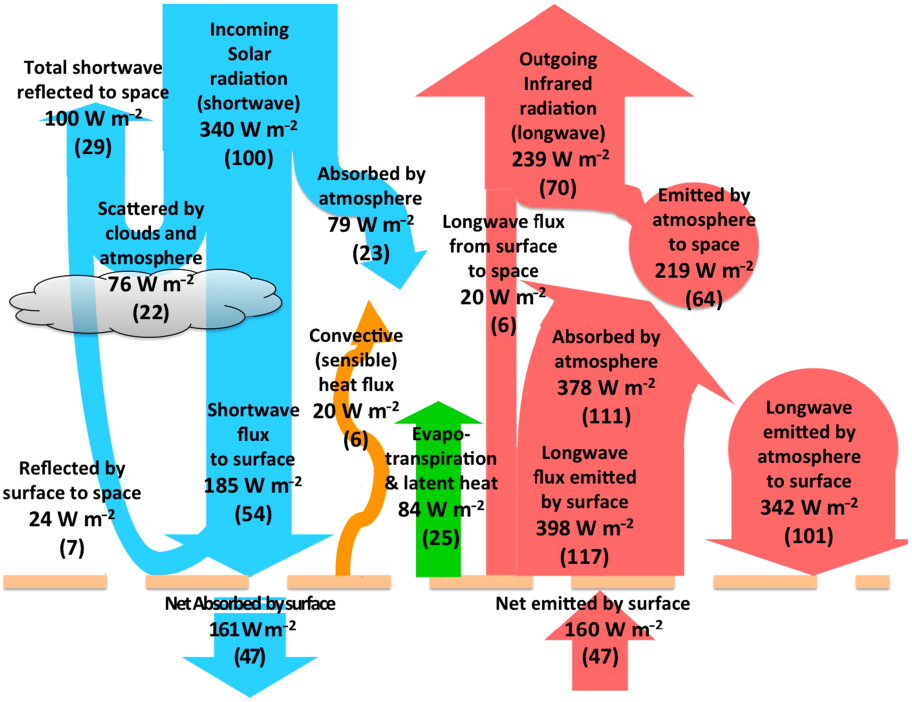

Figure 1. Schematic flow of energy within the Earth's climate system, as determined from a combination of satellite measurements (*ERBE*, *CERES*) (Harrison *et al.*, 1990; Wielicki *et al.*, 1996) and model reanalyses (Trenberth *et al.*, 2009; Kim and Ramanathan, 2012; Stephens *et al.*, 2012; Wild *et al.*, 2013). Solar radiative fluxes are shown on the left (in blue online) and infrared fluxes on the right (salmon pink online); convective and latent heat fluxes are in the centre (in orange and green online). The horizontal dashed line represents the planetary surface. Figures quoted here were based on those obtained by Wild *et al.* (2013) and adapted for the IPCC AR5 report (IPCC, 2013).

energy flow in both the visible/UV and thermal infrared. Incoming solar energy is partly transmitted to the surface, with around 54 dimensionless IPU reaching the ground, the rest being either scattered and reflected back out to space (around 22 IPU due to the atmosphere) or absorbed directly (around 23 IPU, at least partly in the stratospheric ozone layer). Around 7 IPU are reflected from the surface itself back out to space, leaving around 47 IPU actually absorbed at the surface. In the infrared, the atmosphere is relatively opaque, due to the combined effects of various greenhouse gases (H_2O, CO_2, O_3, CH_4, N_2O, etc.) and highly variable clouds and aerosols. This results in the atmosphere absorbing a large fraction (around 95%) of the upwelling radiant flux from the ground (the remainder escaping directly to space), much of which (around 101 IPU or 86% of the upwelling flux from the surface) is re-emitted back towards the surface. The result is a net upward thermal radiative flux from the surface of only around 56 W m^{-2}, amounting to around 16 IPU of the incident solar irradiance. Convection and evapotranspiration amount to an additional upward flux of around 104 W m^{-2} or 31 IPU of the incident solar irradiance, bringing the entire surface budget into approximate balance (although the IPCC AR5 report indicates a small imbalance with a net warming of $\sim$ 0.6 W m^{-2}, potentially associated with changes in ocean heat content). Clouds have a small, but significant and highly variable, contribution, both to latent heat transport and in scattering and absorbing both solar and infrared radiation. Associated uncertainties are thought to be at the level of 5–10 W m^{-2} in each case (e.g. Stephens *et al.*, 2012; Wild *et al.*, 2013). Since the behaviour of their radiative properties and the corresponding impact on precipitation under a changed climate is difficult to predict accurately, this forms one of the key uncertainties in quantifying future climate changes (e.g. see IPCC, 2013).

3. Mars

Mars is arguably the most Earth-like of the other planets of our Solar System. Despite being only around half the linear size of the Earth, with no oceans and a thin atmosphere composed almost entirely of CO_2, it rotates at almost exactly the same rate as the Earth and with an obliquity (25.4°) very similar to that of the Earth. As a result, it exhibits a seasonally varying climate and pattern of circulation that resembles that of the Earth quite closely (e.g. see Read and Lewis, 2004).

3.1. *Data sources*

Mars has also been the subject of intensive exploration, measurement and modelling during the past two decades, with a succession of spacecraft visiting the planet, either in low polar orbit (including the National Aeronautics and Space Administration (NASA) *Mars Global Surveyor*, *Mars Odyssey*, *Mars Reconnaissance Orbiter* and *Maven* spacecraft and European Space Agency (ESA) *Mars Express* orbiter) or *in situ* at the Martian surface (notably NASA's *Pathfinder* and *Phoenix* landers and the *Spirit*, *Opportunity* and *Curiosity Rover* spacecraft). Several of the orbiting spacecraft were equipped with sophisticated remote sensing instrumentation capable of measuring and mapping surface and atmospheric thermal structure, composition, clouds and mineral dust aerosols (e.g. Christensen *et al.*, 2001; Smith *et al.*, 2003; Wolff *et al.*, 2006; Forget *et al.*, 2009; Wolkenberg *et al.*, 2009; McCleese *et al.*, 2010). Use of low altitude, short-period ($\sim$ 2 hourly) polar orbits has allowed some of these spacecraft to obtain synoptic daily maps of atmospheric structure and composition over several Mars years, enabling the development of a quite well-characterized climatology (e.g. Montabone *et al.*, 2015).

Modelling efforts have kept pace with these observational developments, resulting in several groups across the world developing fairly comprehensive global and limited area mesoscale numerical simulation models that capture many features of the observed circulation and meteorology realistically, including the main weather systems, thermal tides, dust storms and clouds (e.g. Haberle *et al.*, 1993; Forget *et al.*, 1999; Newman *et al.*, 2002; Basu *et al.*, 2004; Wilson *et al.*, 2008), at a level of sophistication that rivals Earth climate models in several respects. Such models have demonstrated the capability of reproducing climatological phenomena with an accuracy of a few K in temperature and a few % in horizontal wind velocities and can

also capture various aspects of the dust and condensible transport cycles (of water and CO_2). Together with the availability of spacecraft observations with frequent global coverage, this has led recently to the development and successful implementation of data assimilation techniques to produce 'reanalysis' products for Mars that begin to emulate the capabilities of Earth reanalyses such as those from ERA-40 or the National Centers for Environmental Prediction (NCEP: Montabone *et al.*, 2006; Lewis *et al.*, 2007; Greybush *et al.*, 2012; Montabone *et al.*, 2014). Despite these developments, however, hardly any attempts have appeared in the literature so far to produce quantitative and complete analyses of the Martian global energy budget. The following analysis is therefore arguably long overdue.

For the present analysis, we make use of the European Mars Climate Database (version 5.0) (Lewis *et al.*, 1999, see also http://www-mars.lmd.jussieu.fr), which comprises a set of climatological statistics derived from comprehensive global climate model simulations using the Mars Global Climate Model (GCM) of the Laboratoire de Météorologie Dynamique (LMD) du Centre National de la Recherche Scientifique (CNRS), Paris, developed in collaboration with groups at Oxford University and The Open University in the UK and Instituto de Astrofisica de Andalucia, Spain. To produce this database, the model was run for several Mars years, following a period of equilibration, in order to collect and compile statistics of the atmospheric circulation and meteorology on diurnal, seasonal and interannual time-scales. The model simulations also include detailed calculations of radiative transfer in the visible/UV and thermal infrared throughout the atmosphere, taking account of seasonal variations in the amount of dust suspended in the atmosphere, which have been tuned and verified against a substantial range of the observations from orbit and surface landers. In order to elucidate some other aspects, notably in relation to multiple scattering within dust layers, which is represented relatively crudely in typical GCM radiation schemes for Mars (e.g. Forget *et al.*, 1999) or other planets, we have also included results of some new and detailed radiative calculations using the Non-linear optimal Estimator for MultivariatE spectral analySIS (NEMESIS) radiative transfer tool (Irwin *et al.*, 2008). This is a detailed radiative transfer code that takes a fuller, more accurate and spectrally resolved account of scattering effects than is feasible within the MGCM. The NEMESIS model can compute spectra either using a line-by-line radiative transfer model or the method of correlated-*k*. Multiple scattering is accounted for with a doubling/adding scheme after Plass *et al.* (1973). In these calculations, we used the correlated-*k* method, in which a Gauss–Lobatto quadrature scheme with five ordinates was used to integrate over zenith angle. Although spacecraft measurements have not so far concentrated on measuring the Martian energy budget in detail, temperatures within the MGCM and assimilated analyses (Montabone *et al.*, 2006, 2014) are generally consistent with observations to an accuracy of around ± 3–4 K at low altitude with possible biases of up to 2 K (e.g. Montabone *et al.*, 2006), suggesting an uncertainty in infrared fluxes of around 6–12% or 6–12 W m^{-2}.

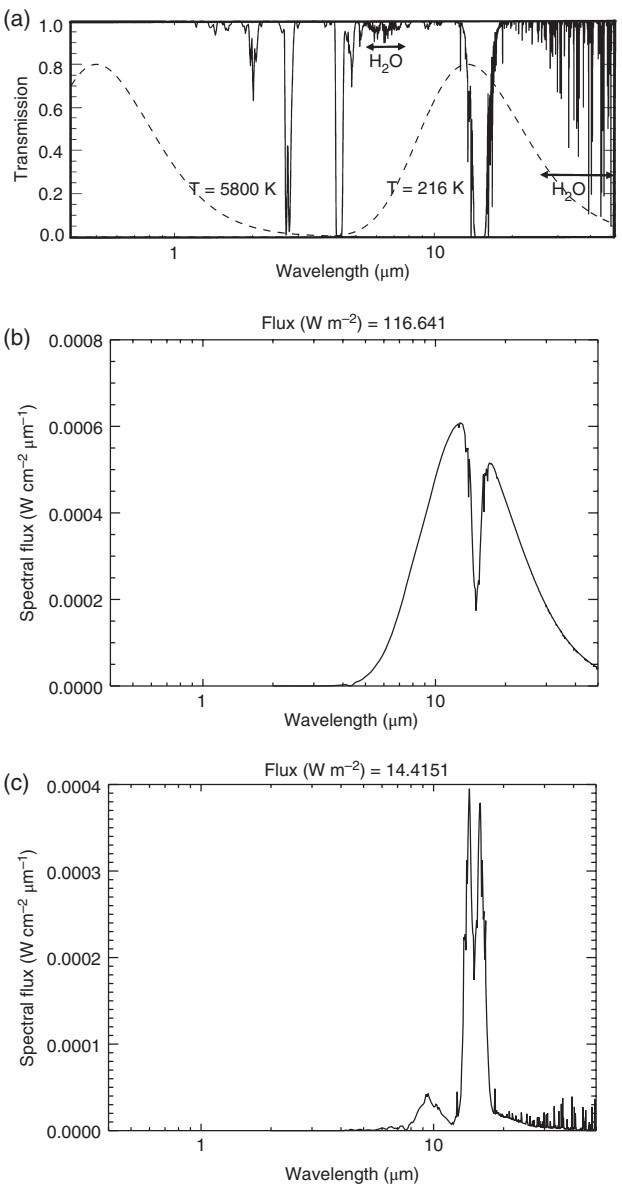

Figure 2. (a) Transmission spectrum at the Martian surface, assuming the COSPAR Martian standard atmosphere temperature profile and composition and neglecting the effects of atmospheric dust. Normalized blackbody curves for $T = 5800$ and 216 K are superposed as dashed lines to indicate parts of the spectrum dominated by solar radiation and infrared emission from the Martian surface. (b) Emission spectrum at the top of the Martian atmosphere, assuming the same atmospheric conditions as in (a), though with a uniform layer of mineral dust confined to the lower atmosphere; (c) emission spectrum at the top of the atmosphere assuming the same atmospheric structure and composition as in (b) but without emission from the surface. Peaks in emission associated with the 15 μm CO_2 band and dust emission around 9–10 μm can be clearly seen. Spectra were computed using the NEMESIS radiative transfer code (Irwin *et al.*, 2008, see text).

3.2. *Energy balances at low dust*

Transmission and absorption of radiation within the Martian atmosphere is somewhat more straightforward to compute than for the Earth, at least in the absence of dust and aerosols (see Figure 2). Gaseous opacity in the visible and near-infrared is influenced only weakly by weak bands of CO_2, but the atmosphere is otherwise almost transparent apart from the effects of Rayleigh scattering. In the thermal infrared, gaseous absorption is dominated by the 15 μm band of CO_2, the centre of which is largely saturated at the Martian surface (see Figure 2(a)), with some weaker (usually unsaturated) lines of H_2O absorption in the mid–far-infrared. Other absorption bands due to CO_2 occur within the 2–5 μm range but the solar and surface blackbody spectra at these wavelengths are relatively weak, so these bands have little impact on energy absorption or emission in this part of the spectrum. This is not unduly surprising, since the Martian atmosphere is relatively very dry (with atmospheric vapour column amounts typically comprising a few tens of precipitable microns of liquid water, representing the layer depth of liquid water if all the water vapour contained within the atmospheric column were extracted, compared with several precipitable cm of liquid water on Earth). However, the Martian atmosphere actually contains a lot more CO_2 than the Earth's atmosphere (around 150 kg m^{-2} on Mars compared with only around 4 kg m^{-2} on Earth), despite the much lower surface pressure of the former. Even so, because the opacity of CO_2 is concentrated into the relatively narrow 15 μm band, it does not actually end up

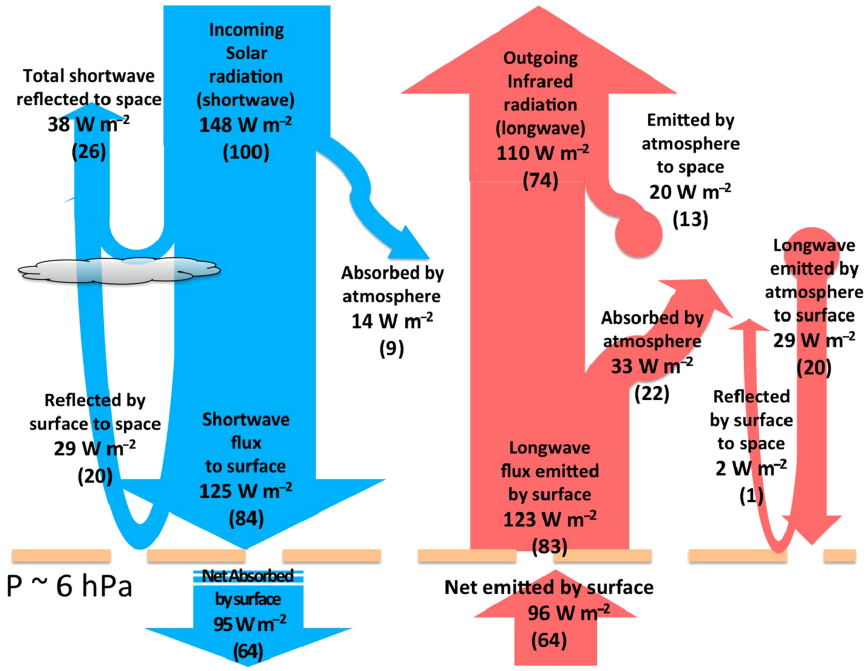

Figure 3. Schematic flow of energy within Mars's climate system, as determined within the ESA Mars Climate Database (Lewis *et al.*, 1999, http://www-mars.lmd.jussieu.fr) Version 5.0 under relatively low dust conditions . As in Figure 1, fluxes are averaged over the globe and over the planetary orbital period. Solar radiative fluxes are shown on the left (in blue online) and infrared fluxes on the right (salmon pink online). The horizontal dashed line represents the planetary surface.

absorbing as large a fraction of the upwelling blackbody emission from the Martian surface as is the case on Earth, when the full range of greenhouse gases is taken into account.

This is clearly illustrated in Figure 2(b) and (c), which show computed spectra for typical emission at the top of the Martian atmosphere under reasonably clear conditions, (b) including and (c) excluding the emission from the surface. Absorption in the 15 μm band evidently removes only a small part of the ∼ 216 K blackbody spectrum from the surface. Correspondingly, the atmosphere itself only emits weakly in the two bands of the spectrum near the 15 μm CO_2 band and a variable band around 9 μm associated with silicate-dominated mineral dust.

The relative transparency of the Martian atmosphere under low dust conditions is clearly reflected in the global energy budget shown in Figure 3. With a dust visible optical depth of around 0.1, more than 80 IPU of the incident solar radiation reaches the surface, with just 9–10 IPU being absorbed on the way down and around 20 reflected back to space from the surface itself (e.g. Christensen *et al.*, 2001; Putzig *et al.*, 2005). As a result, around 64 IPU are actually absorbed by the surface. Even in the infrared, despite the saturated 15 μm band, some 89 W m^{-2} or 60 IPU of the upwelling thermal radiation from the surface reaches the top of the atmosphere and only around 29 W m^{-2} (∼ 20 IPU) is emitted towards the surface from the atmosphere. Hence, the Martian greenhouse warming is relatively modest, amounting to no more than around 5 K at the surface (e.g. Pollack, 1979). Convective (sensible heat) fluxes are generally small compared with the radiative fluxes, so the surface energy balance is well approximated by a direct radiative equilibrium between solar irradiance and thermal emission to space.

3.3. *Seasonal variations*

The orbit of Mars has a large ellipticity = 0.0935, cf.. 0.0167 for the Earth,* so, together with its significant obliquity (25.19°), one might expect the energy budget to be modulated by its seasonal cycle. This is further complicated by systematic variations in the amount of dust suspended in the atmosphere with time of year, such that dust storms and lifting of dust are more active during the perihelion seasons around southern hemisphere summer. This variation is reflected in the level of dust retained in the atmosphere during the course of the model simulations used to compile the Mars Climate Database (Lewis *et al.*, 1999). Figure 4(a) and (b) illustrates how this affects the overall balance of fluxes at the top and bottom of the atmosphere, respectively, for a typical Mars year in which a major planet-encircling dust storm does not occur. The roughly sinusoidal variation in the envelope of upward and downward fluxes with L_S reflects the modulation of insolation as the Sun–Mars distance varies because of the elliptical nature of the orbit. However, the overall distribution of fluxes between the main components does not vary that much during the year, indicating that the annually averaged energy budget shown in Figure 3 remains qualitatively unchanged most of the time, although the absolute amplitudes vary slowly on seasonal time-scales.

Another aspect of the Martian atmosphere that also varies substantially during the year is the rate of condensation of atmospheric CO_2 onto the surface, forming seasonally varying CO_2 ice caps. This has a clearly visible impact on the appearance of Mars during its year, since the condensation of CO_2 during the winter season forms dense polar hood clouds and precipitation of CO_2 snow in layers up to 2–3 m thick in places. Various lines of evidence indicate that around 30% of the entire atmospheric mass is deposited cyclically on to either winter pole during the year (e.g. Hess *et al.*, 1980; Read and Lewis, 2004), so one might expect that this would have a significant impact on the overall energy budget. In practice, however, the latent energy fluxes this condensation produces are relatively very small compared with the radiative energy fluxes. Figure 4(c) shows the seasonal variation of the latent energy flux averaged over the surface area of the planet. This clearly shows a half-yearly cyclic oscillation as each pole accumulates and then evaporates its CO_2 ice cap in turn during the year, with an amplitude of just 1–2 W m^{-2}. This is because, although a large fraction of the atmosphere condenses and evaporates seasonally, the actual absolute amount and rate of condensation are quite small. The rates of condensation and evaporation are essentially determined by a balance between the release or uptake of latent heat of CO_2 (at around 590 kJ kg^{-1}) and radiative heating or cooling. This all takes place on Mars at

*See e.g. http://nssdc.gsfc.nasa.gov/planetary/factsheet/marsfact.html.

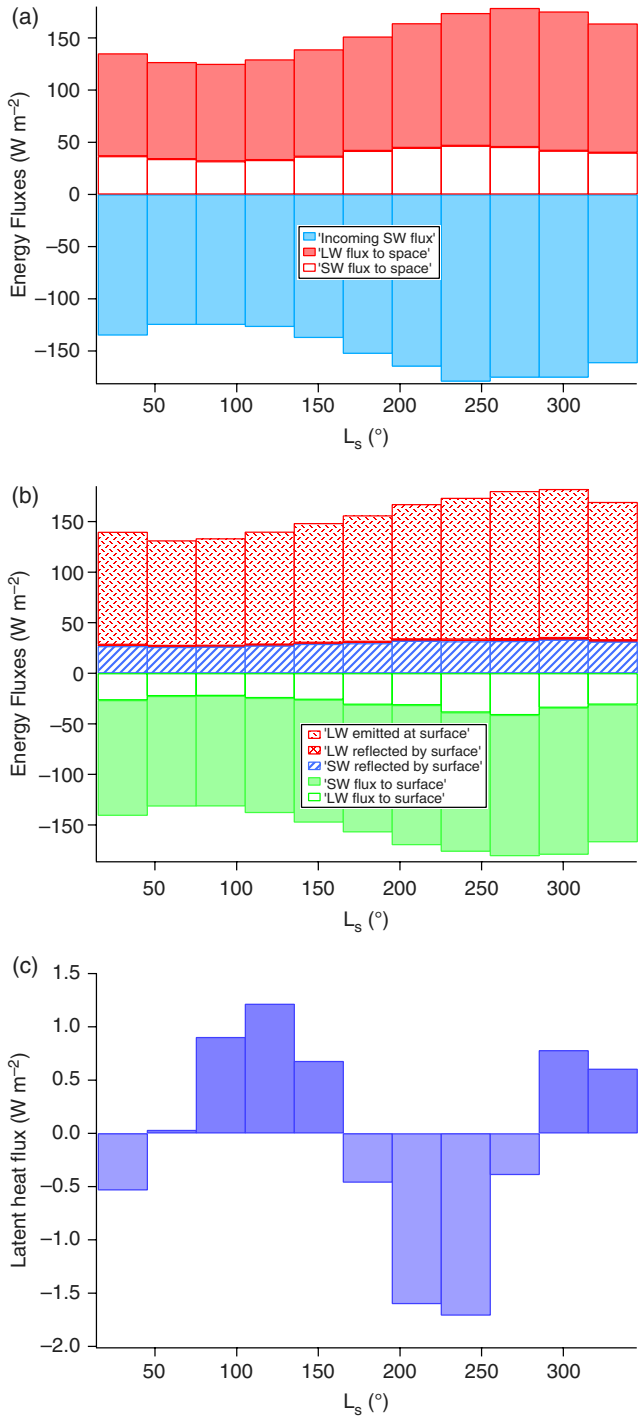

Figure 4. Seasonal variations in the main radiative energy fluxes, (a) at the top of the atmosphere and (b) at the surface of Mars, as computed within the ESA Mars Climate Database (Version 5.0) (Lewis *et al.*, 1999, http://www-mars.lmd.jussieu.fr). Fluxes are averaged over the globe for 12 seasons equally spaced in areocentric longitude L_S. Panel (c) shows the corresponding exchanges of CO_2 latent heat, averaged over the globe for the same seasons as in (a) and (b).

a relatively much lower temperature (around 140–150 K) than it would in the Earth's atmosphere, because of the very low pressures in the Martian atmosphere and at the surface. As a result, latent heat fluxes play only a very small role in the seasonal energy budget, at around the 1% level (despite the large fraction of mass of the atmosphere condensing and evaporating seasonally), in contrast to the Earth, where latent heat fluxes constitute around 25% of the net upward energy flux from the surface (cf.. Figure 1).

3.4. Energy balances during global dust storms

Although most years on Mars are typified by a succession of small local or regional-scale dust storms, interspersed with a low level of dust raising by small-scale convective phenomena such as 'dust devils', every 3–5 Mars years a much larger dust storm event (or events) occurs. In many cases, a number of regional dust storms may effectively coalesce, lifting large amounts of dust that get entrained into the global circulation and are transported to high altitudes over a large fraction of the planet. This typically occurs not too far from the time of perihelion, when insolation levels are near their highest, and individual planet-encircling storm events can lead to global mean visible dust opacities significantly greater than 1 (often up to 5 or even greater). The lifted dust may remain suspended in the atmosphere for several months at a time, so such events may be expected to have a major impact on the global energy budget during this time.

A typical breakdown of the energy budget under such conditions is illustrated in Figure 5, in which a MGCM simulation has been run with prescribed levels of visible dust optical depth τ_v up to 5 (cf. Lewis *et al.*, 1999). This clearly shows major changes in the flow of energy through the atmosphere and to and from the surface. As one might expect, the increased dust opacity substantially reduces the amount of incident solar irradiance reaching the surface, from 84 IPU at low dust to just 22 IPU of the incident flux. The direct solar beam to the surface is, of course, attenuated much more than this at $\tau_v = 5$, but this is offset by the effects of multiple scattering by the dust into diffuse radiation, colouring the sky a reddish brown. In this case, more than half of the incident solar irradiance is absorbed directly by the dust layer in the atmosphere, causing local heating at altitude, a further 24 IPU being scattered and reflected by the dusty atmosphere back out to space. In turn, much less solar energy is absorbed at the surface itself (around 17 IPU), leading to a tendency for the surface to cool compared with clearer conditions.

In the infrared, dust will also increase absorption of upward flux from the surface, but dust is less absorbing at long wavelengths than in the visible, so the impact on the energy budget is less extreme. Scattering also plays a role in the infrared, leading to only around 7–10 W m^{-2} escaping directly to space from the surface. However, dust does increase the amount of diffuse thermal radiation being emitted from the atmosphere to the ground, tending to offset some of the cooling tendency associated with the reduced intensity of sunlight reaching the surface. The overall effect of the increased dust loading is to create an anti-greenhouse effect, warming the upper atmosphere but cooling the surface, which overwhelms the gaseous greenhouse warming during such dust storm events.

This is important in the life cycle of such dust storm events, since the cooling of the surface created by the anti-greenhouse effect will tend to reduce surface winds, as well as shutting off convection in the boundary layer, thus reducing (or even eliminating) surface dust lifting. By this means, the dust storm saturates in amplitude and will start to decay as previously lifted dust begins to sediment to the surface. After around 50–80 days, much of this dust settles to the ground, recovering the more typical clear conditions.

4. Venus

Venus is the other near neighbour to the Earth. In many ways, Venus is even more like the Earth than Mars. The solid planet is almost the same linear size as the Earth and composed of similar materials. Its atmosphere and circulation, however, are radically different from those of the Earth. The Venus atmosphere is much more massive than the Earth's, composed mostly of CO_2 with a surface pressure of around 90 bar, with about the same amount of N_2 and Ar as Earth. Venus's rotation is also radically different from Earth, with a period of around 240 Earth days relative to a frame fixed with respect to the distant stars, but with an obliquity which is effectively nearly 180°, since it rotates retrograde with respect to its orbit. This places the Venus atmospheric circulation in a very different regime from that of

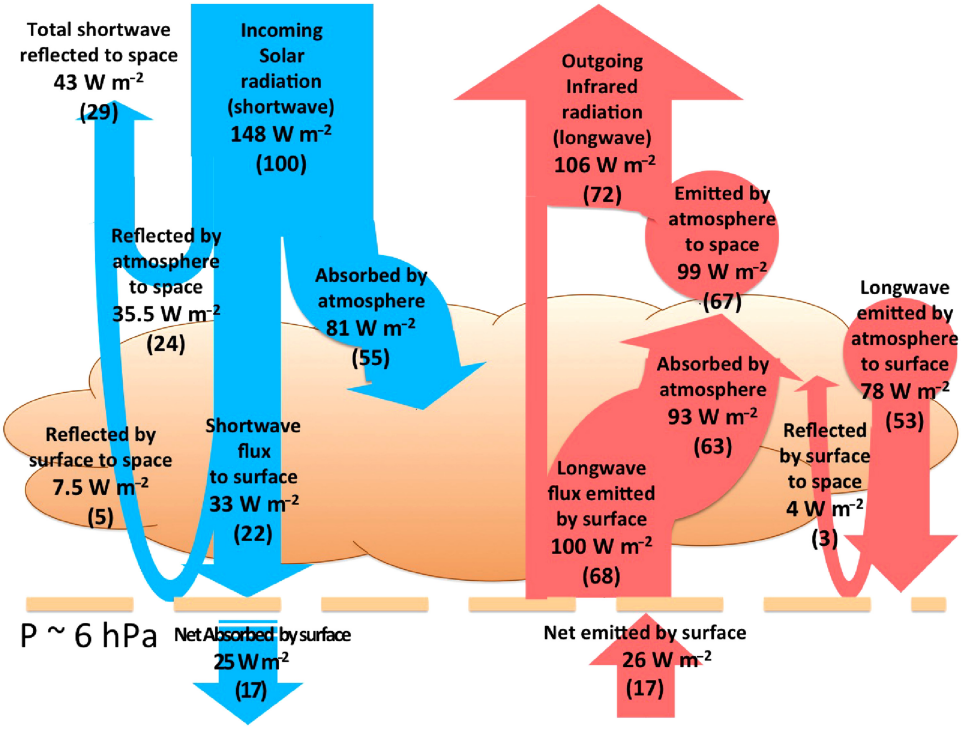

Figure 5. Schematic flow of energy within Mars's climate system, as determined within the ESA Mars Climate Database (Lewis *et al.*, 1999, http://www-mars.lmd.jussieu.fr) Version 5.1 under relatively high dust conditions during major dust storms. As in Figure 1, fluxes are averaged over the globe and over the planetary orbital period. Solar radiative fluxes are shown on the left (in blue online) and infrared fluxes on the right (salmon pink online). The horizontal dashed line represents the planetary surface.

the Earth, with strongly prograde, cyclostrophic zonal winds on the Equator and at midlatitudes and intense and highly variable polar vortices (see e.g. Limaye and Rengel, 2013; Read, 2013). The strongest winds are found in Venus's middle atmosphere at altitudes of around 50–70 km above the surface, close to the tops of dense layers of clouds thought to be composed mostly of sulphuric acid droplets. Winds in the deep atmosphere are comparatively weak and in a circulation regime that appears to be somewhat distinct from that prevailing in the middle and upper atmosphere.

From the viewpoint of the vertical flow of radiant and thermal energy within and through the atmosphere, the distinctive feature is that of an immense greenhouse warming. Despite being significantly closer to the Sun and hence having a solar irradiance at the top of the atmosphere that is more than twice that incident on the Earth, its clouds are highly reflective, so its atmosphere retains less net downward solar flux than the Earth. However, the massive CO_2 atmosphere is strongly opaque in the infrared, even though this opacity is, as on Mars, provided mostly from CO_2 absorption. With such a large CO_2 column ($\sim 10^4$ times that on Mars and $\sim 4 \times 10^5$ times that on Earth) and high surface pressure, even weak spectral lines in the infrared spectrum are significant and the main lines are strongly pressure-broadened. As a result, the observed surface temperature on Venus is around 730 K, compared with its radiative equilibrium temperature of around 230 K.

4.1. *Data sources*

Despite its comparative nearness to Earth, Venus has been visited by robotic spacecraft much less frequently during the past 30 years than has Mars. Even so, there have been missions suitably equipped with instrumentation to measure radiative fluxes at the top of Venus's atmosphere, including NASA's *Pioneer* Venus orbiter (1978–1980) and ESA's *Venus Express* (2006–present). Together with Earth-based astronomical measurements in the visible, UV and infrared, these orbiter missions have provided much information on the cloud-level atmospheric structure and energetics. Deeper levels are relatively inaccessible to remote sounding from space (except in a few narrow spectral windows in the near- and mid-infrared), but some information on radiative fluxes has been obtained by the Russian *Venera* and NASA *Pioneer* Venus entry probes (see e.g. Seiff *et al.*, 1980; Avduevskiy *et al.*, 1983; Revercomb *et al.*, 1985). The overall picture these provide of Venus's atmospheric energy budget have been reviewed in some detail e.g. by Titov *et al.* (2013) and discussed further in the context of a schematic energy budget by Schubert and Mitchell (2013). However, it is not clear how representative of the entire planet the measured fluxes are, since with a small number of probes (which typically can survive only a few hours at the high temperatures in the deep atmosphere) it is only feasible to sample a limited range of latitudes and times of the solar day. Moreover, uncertainties in even the best directly measured radiative fluxes on Venus are generally quite large (Titov *et al.*, 2013), so the Venus energy budget is not very tightly constrained by observations.

For the present study, therefore, we have made use of a numerical radiative–convective model that is used by a new and reasonably comprehensive Venus GCM (Mendonça, 2013; Mendonça *et al.*, 2015). The radiative transfer scheme represents absorption and multiple scattering by gases and clouds using a delta-Eddington/adding method for radiation coming from the Sun and an absorptivity/emissivity formulation for thermal radiation. This enables reasonably accurate computations of radiative fluxes and heating rates, even under extreme Venus conditions, which compare well in precision with much higher spectral resolution calculations (Crisp, 1985; Lee and Richardson, 2011; Mendonça *et al.*, 2015). To produce the global average quantities, the radiative solar fluxes were angularly integrated over a spherical hemisphere using a Gauss–Legendre quadrature method, eight-point rule, during the 1D radiative–convective model integration. The model simulations were typically run until the temperature tendency at all altitudes became sufficiently small (less than 0.001% for a period of 10 Venus solar days). The resulting temperatures and energy fluxes agree with available observations to around ±10%, although the time and space variations of these quantities

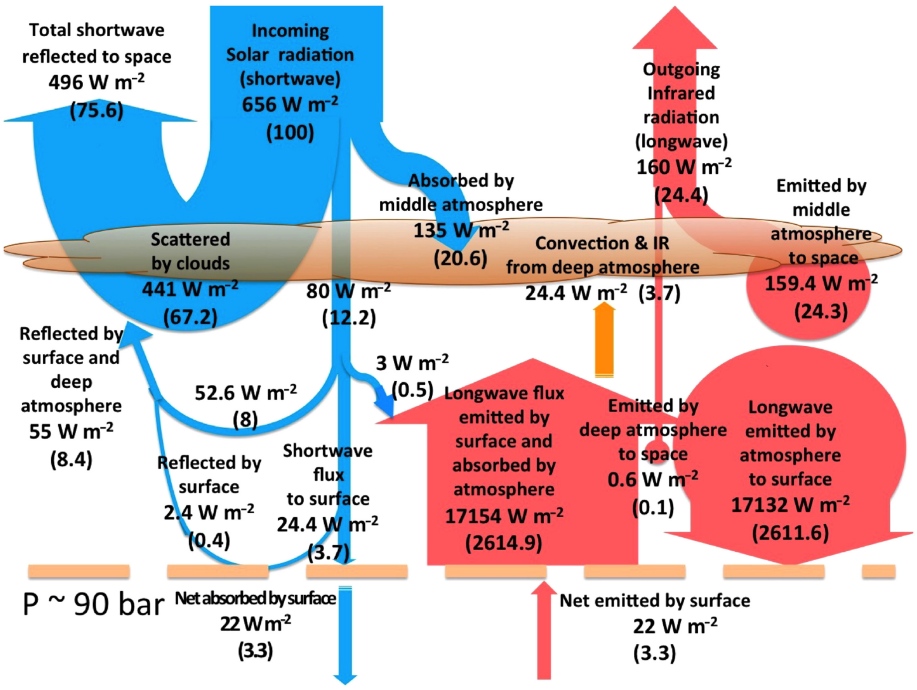

Figure 6. Schematic flow of energy within Venus's climate system, as determined from radiative–convective model simulations (Mendonça, 2013; Mendonça *et al.*, 2015, see text). Solar radiative fluxes are shown on the left (in blue online) and infrared fluxes on the right (salmon pink online); middle atmosphere convective fluxes are to the right of centre (in orange online). The horizontal dashed line represents the planetary surface.

are not well constrained by observations. The energy budget presented below should therefore be seen as a plausible scheme that is internally self-consistent and representative of a reasonably good radiative–dynamical model of the Venus atmosphere in equilibrium.

4.2. *Global energy balances*

The overall globally averaged flow of radiative and thermal energy through the Venus atmosphere in Mendonça *et al.*'s model is summarized in Figure 6. From this, it is clear that the cloudy atmosphere within the middle atmosphere processes the majority of the incoming solar irradiance, with the clouds (at ~ 60 km altitude) reflecting nearly 70% of the incoming radiation straight back to space with a small contribution (~ 8 IPU) scattered from the deep atmosphere (mainly via Rayleigh scattering by CO_2 and N_2 molecules) and the surface. Around 17 IPU of the incoming solar flux is directly absorbed in the middle atmosphere itself, amounting to more than 130 W m^{-2}, with a further ~ 3 W m^{-2} being absorbed by the deep atmosphere. As well as differentially heating the Tropics compared with the polar regions, this absorbed solar flux also drives a strong day–night thermal contrast that excites migrating thermal tides within and above the cloud layers, which play a major role in driving the atmospheric zonal winds and super-rotation in the Tropics. Only a very small fraction (3.7 IPU or 24 W m^{-2}) of the incoming solar irradiance actually reaches the surface when averaged over the globe. This value is in agreement with observational estimates, which suggest a value of around 20 W m^{-2} (Tomasko *et al.*, 1980; Titov *et al.*, 2013).

In the infrared, the upward and downward fluxes at the surface are spectacularly large at more than 17 kW m^{-2}, consistent with the very high blackbody temperatures at these levels. The equilibrated surface temperature simulated in the model is 742 K, which is a consistent value compared with the ones observed by the descent probes (Seiff *et al.*, 1980) of 736 $\pm$6 K. However, the upward and downward long-wave fluxes almost balance by themselves, leaving just a small imbalance of 22 W m^{-2} that is straightforwardly covered by the small residual downward solar flux. At the top of the atmosphere, the cloudy middle atmosphere radiates around 160.1 W m^{-2} to space, supplemented by just 0.6 W m^{-2} that is emitted from the deep atmosphere and surface and is transmitted via the narrow spectral window regions in the infrared. The middle atmosphere energy budget is closed by an upward flux of around 24.4 W m^{-2} (3.7 IPU) from the deep atmosphere, which is partly due to upwelling infrared radiation and partly carried by convection of sensible heat. The fraction carried by convection is somewhat uncertain and model-dependent, but may range from ~ 5–10 W m^{-2} (see also Lebonnois *et al.*, 2015).

Thus, we see that Venus lies in an extreme opposite state to Mars with respect to its energy budget, with most of the energy exchanges taking place in the middle atmosphere and with the deep atmosphere and surface acting almost as a separate and relatively passive 'ocean'. This is also reflected in the pattern of circulation in the atmosphere, though the way in which the deep and middle atmospheres interact dynamically is still not fully understood (e.g. Read, 2013).

5. Titan

Titan is the largest moon of Saturn and is the only natural satellite of another planet known to host a substantial atmosphere. Titan itself is a body around the size of the planet Mercury or 50% larger than the Earth's moon, though is almost certainly composed of a mixture of rock and ices, which gives it a mean density of only 1.88×10^3 kg m^{-3}. It hosts a relatively deep atmosphere composed mostly of N_2 and small amounts of CH_4 and other hydrocarbons that, with a mean surface pressure of 1.45 bar, is actually more massive than that of the Earth. Like many of the larger moons of the gas giant planets, the rotation of Titan itself is tidally locked to its orbit around Saturn, with a period of 15 days 23 h. Thus, its atmospheric circulation regime is somewhat similar to that of Venus in forming strongly super-rotating, global cyclostrophic zonal winds with intense polar vortices. The atmosphere is seen to be largely covered by a deep though tenuous layer of haze, composed of photochemically produced aerosol particles thought to include tholins and complex organo-nitrogen compounds (e.g. Atreya *et al.*, 2006).

From an energy budget viewpoint, Titan's atmosphere is very weakly irradiated by the Sun at the orbit of Saturn, with a mean solar irradiance of only around 3.7 W m^{-2}. Even so, this is evidently sufficient to drive substantial and energetic motions within the atmosphere and to sustain an analogue of Earth's hydrological cycle, though involving methane in its vapour and liquid forms (including the formation of permanent lakes of liquid methane at high latitudes (Stofan *et al.*, 2007; Lunine and Atreya, 2008)). Formation of methane clouds has also been observed, indicating the occasional presence of vigorous convection. Titan's atmosphere is highly extended, because of the moon's relatively low surface gravity, and the atmosphere exhibits both a well-developed troposphere (up to around 50 km altitude) within which temperature falls monotonically with height and a thick stratosphere (up to 250–300 km altitude) where temperature increases with height. This is because its gaseous composition induces a greenhouse warming by virtue mainly of CH_4, whereas its (mostly stratospheric) smoggy haze layer directly absorbs sunlight and produces an anti-greenhouse effect that cools the lower atmosphere. It is logical, therefore, to examine the energy flow within and through Titan's atmosphere by treating the troposphere and stratosphere separately.

5.1. Data sources

Titan has been the subject of intense study since the *Voyager* fly-by mission obtained close-up measurements and images of the satellite in 1982. Many of the observational measurements available were acquired during the *Voyager* fly-by itself and (especially) during the recent orbital tour of the Saturn system by the NASA *Cassini* spacecraft. The latter has been in orbit around Saturn since 2004 and has made a close fly-by encounter with Titan on almost all of its $\sim$ 60 day orbits, allowing the spacecraft to image Titan and to make a wide range of remote sensing measurements of absorption and emission spectra from the UV to the far-infrared and to map its atmospheric properties (see Müller-Wodarg *et al.* (2014) for recent reviews). Such orbital remote sensing measurements across the electromagnetic spectrum were also supplemented in 2004 during the descent and landing of the ESA *Huygens* probe through Titan's atmosphere on to its surface (Fulchignoni *et al.*, 2005; Tomasko *et al.*, 2008). In addition, Titan has been observed intermittently from the Earth by a variety of astronomical instruments and telescopes, especially during the *Cassini* era, culminating in the observational study of Titan's global energy budget by Li *et al.* (2011) using extensive measurements from the Composite Infrared Spectrometer instrument on the *Cassini* orbiter. These measurements indicated an outgoing mean radiative flux at the reference altitude of 250 km of 2.83 ± 0.01 W m^{-2} and a net imbalance with incoming solar radiation of no more than 6%.

Such a wealth of measurements has also been complemented by an intensive set of modelling studies, ranging from 1D radiative–convective equilibrium models using reasonably complex radiative transfer schemes (e.g. McKay *et al.*, 1991) to more complex 3D global circulation models (Hourdin *et al.*, 1995; Rannou *et al.*, 2004; Lebonnois *et al.*, 2012; Mitchell, 2012). These have allowed a careful decomposition of Titan's atmospheric energy budget at varying levels of detail. Indeed Titan was one of the first non-terrestrial planets about which a Trenberth-style energy budget diagram was constructed (McKay *et al.*, 1991), mainly to illustrate how its greenhouse and anti-greenhouse warming and cooling operated.

The analysis we present here is still largely based on the early study of McKay *et al.* (1991). However, more recent modelling studies (Charnay and Lebonnois, 2012; Mitchell, 2012; Schubert and Mitchell, 2013) have highlighted a likely deficiency of the analysis by McKay *et al.* (1991) in underestimating the intensity of atmospheric convection and dynamical transport. The observed formation of rapidly varying methane clouds during Titan's spring and summer (Rodriguez *et al.*, 2011; Turtle *et al.*, 2011) suggests that tropospheric convection and horizontal heat transport are more intense that had been apparent in McKay *et al.*'s radiative–convective equilibrium model. As a result, estimates of the sensible and latent heat fluxes near the surface needed to be revised, with corresponding adjustments in other aspects of the tropospheric heat budget to describe the equilibrium. The resulting TOA energy fluxes are consistent with the measurements of Li *et al.* (2011) to within a few per cent, although the internal and surface fluxes are not well constrained by observations.

5.2. Global energy balances

Figure 7 summarizes the main energy transfers between the surface, troposphere, stratosphere and space, based on the fluxes computed from Titan GCM simulations using the model of Charnay and Lebonnois (2012). As in previous sections, we show the fluxes both in terms of absolute energy fluxes (in W m^{-2}) and normalized with respect to the incoming solar irradiance. The figures from the LMD model compare quite closely with those of McKay *et al.* (1991), Williams *et al.* (2012) and Mitchell (2012) although, as also noted by Mitchell (2012), the inclusion of effects associated with convection and horizontal transport in the GCM simulations makes a significant difference to several of the results, with convection making a greater contribution to the upward near-surface fluxes than in the radiative–convective calculations of McKay *et al.* (1991).

From Figure 7, it is clear that around 52 IPU of the incoming solar irradiance is absorbed in Titan's stratosphere, mainly due to its orange smog/haze, while around 21 IPU is directly scattered back out to space within the stratosphere. The remaining solar energy makes it into the deep troposphere, where around two-thirds ($\sim$ 17% of total solar irradiance) is absorbed within the troposphere itself and the remaining third ($\sim$ 9 IPU) reaches the surface. A small amount of that is reflected back out to space (mainly due to Rayleigh scattering), leaving around 0.25 W m^{-2} to be absorbed directly by the surface itself and 0.08 W m^{-2} to be reflected. The upward convective heat flux predicted by the Titan IPSL GCM amounts to around 60% of the solar flux absorbed at the surface (Charnay and Lebonnois, 2012), close to (though somewhat smaller than) the 8 IPU estimated by Mitchell (2012). In the infrared, the relatively opaque troposphere (due largely to CH_4–N_2 H_2–N_2 and N_2–N_2 collision induced absorption: e.g. see McKay *et al.*, 1991) emits around 10% more energy to the surface than Titan receives from the Sun, consistent with a positive greenhouse warming. As a result, its surface warms to a significantly higher temperature than Titan's radiative equilibrium temperature, emitting 113 IPU of solar irradiance upward from the surface, also helping to maintain the warm troposphere. In the stratosphere, however, infrared emissions to space are weaker than the absorbed solar fluxes, consistent with Titan's stratospheric anti-greenhouse effect. This leads to a net warming of Titan's upper stratosphere at the expense of the tropopause, leading to the development of an increasing temperature with height, somewhat as observed in the Earth's ozone layer (which can also be regarded in certain respects as exhibiting an anti-greenhouse effect).

Hence, we see that the energy budget of Titan's atmosphere has features in common with both Venus and the Earth. High-level clouds and hazes on both Venus and Titan lead to significant energy exchanges in their middle atmospheres, including both strong scattering and absorption of solar energy, which drives a vigorous atmospheric circulation (this is the altitude where super-rotating zonal winds reach their peak). The troposphere of Titan, however, operates more like that of the Earth, with a strong greenhouse warming (with CH_4 and H_2 playing the role on Titan of, respectively, H_2O and CO_2 on Earth) and an active hydrological cycle with occasional episodes of convective and latent heat transport. A major quantitative difference, of

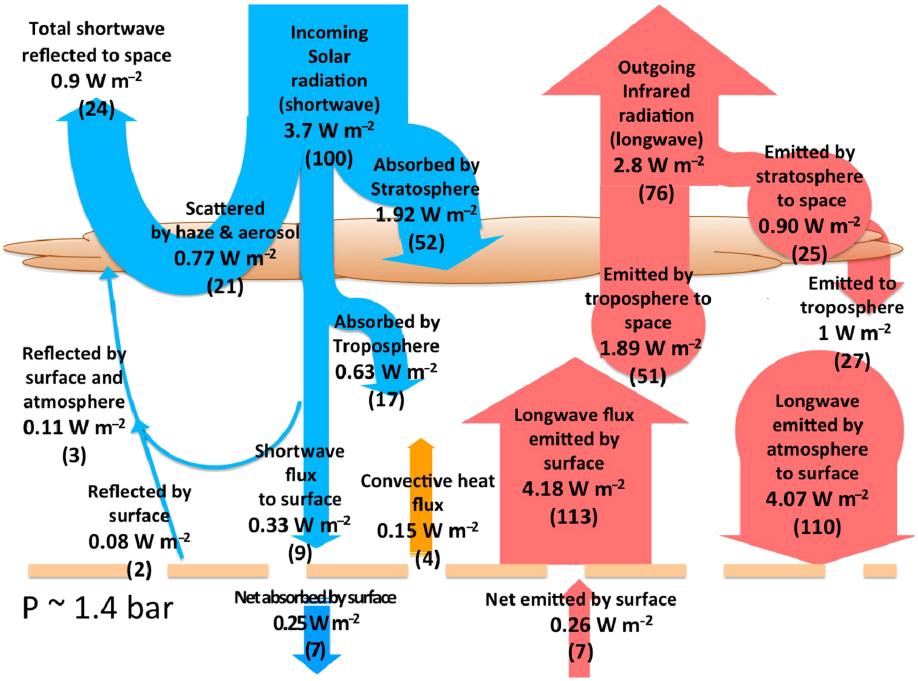

Figure 7. Schematic flow of energy within Titan's climate system, as determined from radiative–convective and general circulation model simulations (McKay *et al.*, 1991; Charnay and Lebonnois, 2012; Mitchell, 2012). Solar radiative fluxes are shown on the left (in blue online) and infrared fluxes on the right (salmon pink online); convective fluxes are in the centre (in orange online). The horizontal dashed line represents the planetary surface.

course, is that Titan maintains such active energy transport and meteorology with a relatively tiny throughput of energy in absolute terms compared with Earth and Venus.

6. Jupiter

Atmospheric energy budgets for gas giant planets such as Jupiter may also be treated in a similar way to the approach adopted here for the terrestrial planets (with rocky surfaces and relatively shallow atmospheres), at least in principle, although some features need to be redefined carefully. This is partly because, unlike terrestrial planets, gas giant planets do not have a well defined surface (solid or otherwise) at which incoming solar irradiance is eventually absorbed and heated. Instead, incoming solar energy is gradually scattered and absorbed with increasing depth until it is essentially exhausted. In addition, most gas or ice giant planets in the Solar System are observed to be net emitters of thermal radiation, indicating that they retain an interior source of energy that, in the cases of Jupiter, Saturn and Neptune, is of comparable strength to the solar irradiance itself. This interior energy source in the case of planets the size of Jupiter is not due to nuclear energy generation but is more likely associated with the slow release of gravitational potential energy as the entire planet shrinks and cools from its initially hot primordial state (Hubbard, 1968, 1977). This suggests a concentration of released gravitational energy as a source of heat where the density is highest, in the deep interior, which is thus likely to energize statically unstable convection over much of the fluid interior of the entire planet (e.g. Guillot *et al.*, 2004).

Thus, an initial question to be resolved is where to define the base of the domain over which an energy budget can be computed? For Jupiter and similar 'cold' gas giants (by which is meant planets with interior heat sources that are of the same order as the solar/stellar irradiance at TOA), a possible lower boundary for energy budget calculations could be the so-called radiative–convective boundary. This is defined effectively as the level at which the vertical thermal gradient or lapse rate in purely radiative equilibrium first becomes superadiabatic, implying the onset of free convection (Sagan, 1969; Robinson and Catling, 2012, 2014), and effectively corresponds to the location where the local downward solar flux becomes comparable with the upwelling convective heat flux from the deep interior. In practice, however, this typically corresponds to a relatively shallow depth below the tropopause (at around 0.5–1 bar pressure in the case of Jupiter), below which solar irradiance continues to be absorbed in parallel with upwelling infrared radiation.

A more satisfactory boundary for tropospheric energy budget calculations (and the one used here) is taken to be the shallowest depth (below the tropopause) at which the absorption of incoming solar irradiance is essentially complete. This allows us to draw a boundary below which upward energy transfer is almost entirely convective and above which the transfer of energy is accomplished by a complex mix of convective and radiative heat fluxes. Thus, for simplicity, in the following two sections we consider the vertical transfer of energy at just two levels: (i) at the top of the atmosphere as before and (ii) at the bottom of the 'radiative absorption zone'.

6.1. *Data sources*

The global energy budget of Jupiter has been the subject of intensive study and measurement, ever since its excess of infrared emission over its net solar irradiance was discovered (Low, 1966). Initial measurements were made using wide-bandwidth infrared and visible wavelength observations from the *Voyager* fly-bys in 1979 over a range of phase angles to determine both the visible Bond albedo and the total thermal emission (Hanel *et al.*, 1981). Since then, several other studies have attempted to refine these measurements, combining the original *Voyager* measurements with new observations from the *Cassini* Visual and Infrared Mapping Spectrometer (VIMS) and Composite InfraRed Spectrometer (CIRS) instruments during the 2000 fly-by (Li *et al.*, 2012) to constrain the global TOA outgoing radiative fluxes to a precision of 30 mW m^{-2}, corresponding to around 0.25% of the global energy output. Detailed net radiative flux measurements were also made during the descent of the *Galileo* probe to Jupiter in 1995 (Sromovsky *et al.*, 1998), which allowed a clear determination of the levels to which solar irradiance penetrated within Jupiter's tropical atmosphere. This clearly showed that almost all of the incoming solar flux had been absorbed down

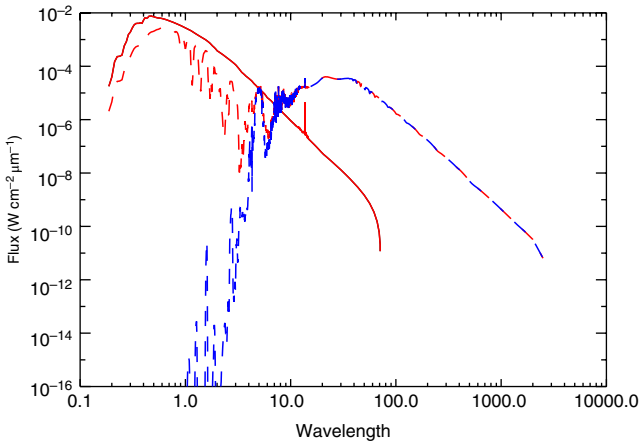

Figure 8. Spectrum of visible and thermal emission from the top of Jupiter's atmosphere, computed using NEMESIS. The solid line indicates the spectrum of the incident sunlight and the (upwelling) scattered component is shown by the light grey (red online) dashed line. The darker (blue online) dashed line indicates the thermal emission spectrum of Jupiter, computed without incident sunlight.

to pressure levels of around 5–7 bar. At this level, the infrared optical depth of the atmosphere is likely to be quite high and so upward heat transfer beneath this level is likely to be dominated by thermal convection, apart from the effects of narrow spectral windows within the infrared, through which radiative transfer from deep levels can occur relatively unattenuated. Radiation from such deep levels is clearly evident, for example, in images taken of Jupiter in the 5 μm infrared band, which delineates regions of thin cloud that allow radiation from deep levels to escape directly to space (e.g. West *et al.*, 2004).

Evaluating the quantitative impact of these spectral window regions and the net absorption of solar and infrared radiation as a function of depth in Jupiter's atmosphere cannot be done easily from observations alone. For the analysis presented here, therefore, we have also made some detailed radiative calculations using the NEMESIS radiative transfer tool (Irwin *et al.*, 2008) to compute spectrally integrated radiative fluxes in a 1D representation of Jupiter's atmosphere. These calculations assumed a standard composition of Jupiter's atmosphere (e.g. Irwin *et al.*, 2005) and took account of the presence of a single cloud layer of ammonia ice, using a typical temperature profile for Jupiter based on observations for $p < 1$ bar and extrapolated to depths of several tens of bar as a simple adiabat. Figure 8 illustrates some results of these calculations in the form of synthetic emission spectra across the visible and infrared wavelength regions for the top of Jupiter's atmospheres. This clearly shows the wealth of lines and continuum features associated with emission from hydrocarbon constituents, collision-broadened lines of H_2 and cloud aerosols. A notable feature is the strong emission around 5 μm wavelength ($\sim$ 2000 cm^{-1} in wavenumber) associated with upwelling radiation from levels deeper than 2–3 bar in this spectral window region. Apart from the isolated 5 μm region, radiation at wavelengths longer than around 10 μm is clearly seen to be due entirely to thermal emission, while at wavelengths shorter than ~7 μm the radiation is from scattered sunlight.

In the following analysis, the NEMESIS calculations were used to decompose aspects of the infrared and visible radiative fluxes that contribute to the total energy budget determined observationally by Li *et al.* (2012) and others. The resulting computed TOA fluxes are consistent with the measurements of Li *et al.* (2012) to within 1–2%, including the contribution from the deep atmosphere in the 5 μm window region, although the latter only amounts to around 2% of the upwelling energy from the deep interior and less than 1% of the global mean energy radiated to space (see below and Figure 9).

6.2. *Global energy budget*

The overall flow of energy within and through the 'radiative absorption zone' of Jupiter (i.e. $p > 3$–5 bar) is presented schematically in Figure 9. At the bottom of this zone, the atmosphere is assumed to be optically thick in the infrared and essentially opaque, with the majority of the $\sim$ 5.7 W m^{-2} upwelling heat energy from the deep interior entering this zone as a convective (sensible heat) flux, though with a small contribution arising from the radiative contribution in the 5 μm thermal

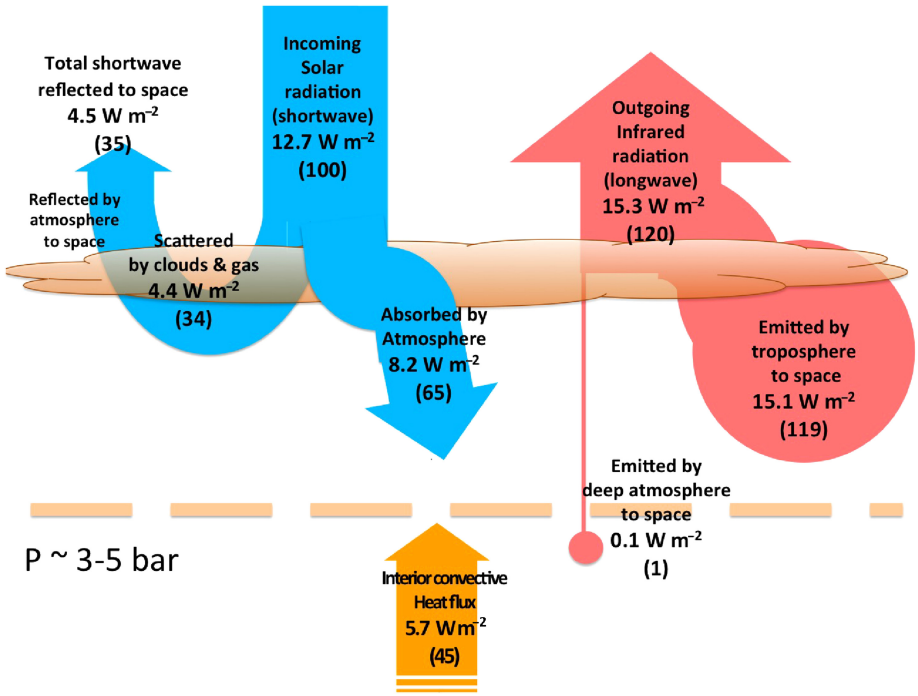

Figure 9. Schematic flow of energy within Jupiter's irradiated troposphere and stratosphere, as determined from a combination of *Voyager* and *Cassini* measurements (Li *et al.*, 2012) and NEMESIS model calculations (Irwin *et al.*, 2008, see text). Solar radiative fluxes are shown on the left (in blue online) and infrared fluxes on the right (salmon pink online); upwelling interior convective fluxes are in the centre (in orange online). The horizontal dashed line represents the approximate boundary in the atmosphere below which solar insolation does not penetrate.

infrared window region of around 100 mW m^{-2}. This emission comes from regions of the atmosphere deeper than 5–10 bar and is quite inhomogeneous across the planet, because it can only emerge in regions where the upper cloud layers are relatively thin. The thicker cloud layers of NH_3 and NH_4SH ice and H_2O are optically thick at 5 μm and so this spectral region only contributes a small amount to the total radiative output of the planet.

At the top of this atmospheric zone, 12.7 W m^{-2} of visible and UV solar radiation is incident upon the stratosphere and upper troposphere at Jupiter's distance from the Sun of ∼ 5 au, of which around a third is scattered back into space through Rayleigh scattering, stratospheric haze particles and (most especially in the troposphere) from the upper cloud layers. Thus, a net total of around 8.4 W m^{-2} or 66 IPU of the incident solar irradiance is absorbed within the stratosphere and upper troposphere. This combines with the upwelling interior heat to provide around 14.1 W m^{-2} of heat input within the radiative absorption zone, which must therefore be re-radiated out to space in equilibrium. By this means, Jupiter appears to radiate around 111 IPU or 68% more energy in the infrared to space than its net input of solar energy.

This style of energy budget is likely to be typical of a whole class of giant planet, in which radiative energy from the parent star combines with internal heat to produce a dynamically active upper troposphere and stratosphere. Such a class would include most of the giant planets in the Solar System with the possible exception of Uranus, which does not appear to have a substantial internal heat source (Pearl *et al.*, 1990). Even so, the same schematic analysis of energy flow should apply, though with the interior convective flux reduced appropriately.

7. 'Hot Jupiter': HD 189733b

In recent years, the census of planets known to exist and retain a substantial atmosphere has grown enormously, following the discovery, detection and characterization (albeit often very rudimentary) by astronomers of planets around other stars. One of the most ubiquitous classes of planet among the 1900 or so extrasolar planets discovered so far (e.g. Schneider *et al.*, 2011) is the so-called 'hot Jupiter' gas giant. Such planets are of comparable size and mass to Jupiter in our own Solar System, but have been found to occur in very close-in orbits around their parent stars. They were among the first extrasolar planets to be discovered because they exert the strongest impact on their parent star, either through gravitational perturbations of the star's motion in space (detected through slowly varying Doppler shifts of the stellar spectral lines) or through direct occultation of starlight by the planet passing in front of (or behind) the star.

Hot Jupiters appear to have a similar composition to the gas giants found in our Solar System, comprising a deep, fluid envelope composed mostly of hydrogen and helium, perhaps with a massive rocky core of comparable size to the Earth (although this is uncertain even for Jupiter; e.g. see Guillot *et al.*, 2004). They are termed 'hot Jupiters' because, at their inferred distance from the parent star (typically ≪ 1 au), the stellar irradiance they receive at the top of their atmospheres is much greater (by orders of magnitude) than the solar irradiance at the Earth's TOA. As a result, atmospheric temperatures in their upper tropospheres may soar to temperatures of order 1000–2000 K or even greater on the day side. Another likely consequence of their very small orbital radius is that tidal forces from the parent star may well result in synchronization of their bulk rotation rate to that of their orbit so, like the Earth's moon, they present approximately the same face to the star all the time. Hence, their 'climate' is typified by two very distinct regimes – a massively hot and energetic day side and a relatively cool night side. A major uncertainty with these planets, however, is the extent to which atmospheric motions are able to transport heat from the hot day side to warm the night side. Hence, scientists are now attempting to apply 3D global circulation modelling techniques to try to develop a theoretical understanding of this process (e.g. Showman *et al.*, 2010).

7.1. Data sources

The present analysis is based on a synthesis of astronomical measurements and radiative transfer model calculations for the hot Jupiter exoplanet HD 189733b. This planet was discovered in 2005 (Bouchy *et al.*, 2005) in close orbit around the star HD 189733, which is a star of K1.5V type, somewhat smaller than the Sun, at a distance from the Sun of around 19.5 pc. It has been the subject of extensive study using both ground-based and space-based astronomical telescopes in both primary and secondary transit (the latter being when the planet passes behind the star relative to the Earth) over a wide range of wavelengths, including the thermal infrared (Knutson *et al.*, 2012). This has enabled a reasonably full light curve to be obtained for this planet, from which not only spectral information but also some indication of variations of atmospheric temperature and outgoing thermal flux in longitude has been obtained.

These measurements have been supplemented further here with some calculations of the day-side and night-side thermal structure and radiative balance using the NEMESIS radiative transfer model (Irwin *et al.*, 2008; Barstow *et al.*, 2014). The incoming stellar flux was calculated based on the Kurucz model[†] for HD 189733. The amount that may be reflected was based on the albedo spectrum presented by Evans *et al.* (2013), but these data do not provide any information beyond the wavelength range 0.3–0.6 μm. Therefore, this number is not tightly constrained.

The outgoing thermal flux was calculated based on a range of models for the day side and night side. The day-side model with the largest amount of outgoing flux is based on the best-fitting results of Barstow *et al.* (2014). Increasing the H_2O abundance to the maximum allowed by Barstow *et al.* (2014) reduces the outgoing flux, while increasing the assumed potassium abundance by a factor of 10 reduces it further. There is very little constraint on the day-side potassium abundance, as no measurements have yet been made between 0.6 and 1.0 μm, where the major potassium band can be observed. The night-side flux was estimated in two different ways, first by adjusting the temperature profile from the best-fitting day-side case and calculating a spectrum based on this atmospheric model and secondly by simply scaling the best-fitting day-side spectrum. Both approaches are compatible with the night-side photometric fluxes presented by Knutson *et al.* (2012).

Due to the lack of measurements on the night side and around the 1 μm region on the day side where, depending on the abundances of alkali metals and the properties of any clouds that may be present, there may be significant or very little thermal flux, each of the fluxes has a wide range of possible values. A major uncertainty in these calculations is the albedo of the planet, due to both gaseous scattering and scattering due to clouds. At the inferred atmospheric temperatures, most condensible substances familiar in colder planets will not form clouds. However, various species such as $MgSiO_3$, metal sulphides, chromium and iron are thought to condense to form clouds at temperatures ranging from 500–2500 K (e.g. Helling *et al.*, 2008; Morley *et al.*, 2012), corresponding to pressures of ∼ 10 hPa up to a few bar. In the present case, the NEMESIS calculations suggest that the majority of the incoming 240 kW m^{-2} stellar irradiance is deposited within the top few bar of the atmosphere of HD 189733b on its day side.

7.2. Global energy budget

The resulting global energy budget for this exotic extrasolar planet is presented in Figure 10, where we have divided the calculations explicitly between the day and night sides of the planet, but the

[†]See http://kurucz.harvard.edu/stars.html

dynamical day–night flux and internal heat source are averaged over the whole planet. At the mean orbital distance of 0.03 au from its parent star, the incident stellar irradiance is actually around 496 kW m^{-2}. When averaged over the day side *only*, this amounts to a mean TOA irradiance of 248 kW m^{-2}, which needs to come into balance with the direct long-wave emission and net heat transport to the night side. Given the observational estimate of between 45 and $\sim$ 115 kW m^{-2} for the mean night-side long-wave emitted flux to space, this suggests that more than 80% of the incoming stellar radiative flux is returned to space on the day side by direct long-wave emission. Up to around one third of the incident flux ($\leq$ 73 kW m^{-2} or $\leq$ 30 IPU) must therefore be transported horizontally by winds within the planet's atmosphere to the night side, finally to be emitted to space as long-wave radiation.

An interesting implication of these results is that the planet appears to emit significantly more energy in the infrared than it receives from its parent star, by at least 7 kW m^{-2} when averaged over the planet (assuming it to be horizontally uniform for simplicity). Minimum and maximum values for the internal heat flux and day–night transport are calculated from the extreme values of the incoming and outgoing fluxes, which are constrained by observation. The internal flux and transport are dependent on each other and cannot be maximized or minimized simultaneously. For example, if the day to night transport is maximized, the incoming day-side flux and outgoing night-side flux both have their maximum values, whilst the outgoing day-side flux is minimized. In this case, the internal heat flux is 42 kW m^{-2} (or 17 IPU), which is approximately half of the maximum value that can be consistent with all constraints.

The presence of a significant interior heat source emanating from within hot Jupiter planets appears to be a relatively common occurrence, although the precise mechanisms responsible for such a flux are not yet well understood. Various suggestions have included the storage at depth of stellar irradiated energy and subsequent release, the dissipation of mechanical energy associated with tidal forces as the orbit and rotation of the planet evolve, or ohmic dissipation associated with strong magnetohydrodynamic flows in the ionized regions of the planet's atmosphere (see e.g. Fortney *et al.*, 2010, for a recent review). Estimates have varied widely over how large such energy sources could be, but the value obtained here ($\gtrsim$ 7 kW m^{-2} or $\gtrsim$ 3 IPU) as a lower limit is relatively high for such objects. In some cases, energy deposition in the interiors of similar planets is thought to lead to a significant 'inflation' of the apparent planetary radius, although this does not seem to be the case for HD 189733b. Nevertheless, this picture is broadly consistent with a number of modelling studies (e.g. Rauscher and Menou, 2013), although there remain many uncertainties as to the mechanisms for how heat may be transported between daytime and night-time hemispheres (see e.g. Showman *et al.*, 2010, and the further discussion in section 8 below).

8. Discussion

In this article, we have brought together and reviewed the results of some of the most recent work on quantifying the global climatological energy budgets for a number of representative planets of our Solar System and beyond. These were supplemented with some new radiative transfer calculations carried out specifically for this article and we have presented them all in a standardized form for direct comparison with the well-known 'Trenberth diagram' for the Earth. This approach demonstrates vividly the usefulness of the 'Trenberth diagram' for summarizing a great deal of complex and sophisticated information in a very compact form, yielding some powerful insights into the way in which an atmosphere influences the flow of energy into and out from the main body of the planet to space and either at its surface (if it has one) or its deep interior.

The utility of the 'Trenberth diagram' has been widely appreciated for many years for the Earth as both a research and educational tool. Its application to other planets has not hitherto been very common, which, in light of the insights presented herein, is somewhat surprising. However, the reasons are not that hard to appreciate. Despite its apparent simplicity in presentation, many of the terms within the global energy budget of a planetary climate system are not easy to quantify accurately, either from measurements or from models. For many planets, measurements of key terms in the energy budget have simply not been available until comparatively recently and even now the range of information available from direct measurements is quite limited. This situation has been evolving rapidly in recent years, however, and certainly for the atmospheres of Mars and Venus quite a large number of measurements have become available from a host of new space missions. Even for Titan and Jupiter, major advances have been made, so that observations now provide significant constraints on most of the key energy exchanges, at least near the tops of their atmospheres. The situation regarding extrasolar planets, however, still has quite a way to go before their climatology can be characterized reliably.

Perhaps the principal advance that has made it possible to construct global energy budgets for planets other than the Earth has been the development of modelling techniques, either through detailed 1D radiative transfer energy balance models that accurately take into account all of the main atmospheric constituents and surface properties or through the emergence of comprehensive 3D global circulation models that incorporate representations of radiative transfers with sufficient accuracy to be consistent with observational constraints. The use of fully 3D models allows the full variability of atmospheric and surface albedo and opacity to be taken into account, in principle enabling a more representative evaluation of long-term energy exchanges within a planetary climate system to be carried out. This has proved possible here for Mars and Titan, although figures for Mars needed to be supplemented by further computations using more detailed radiative transfer models. As a result, we now have enough information available to be able to construct self-consistent energy budgets that are consistent with such observational information as may be available, thus facilitating robust qualitative comparisons with the Earth.

In making such comparisons with the Earth, it is important to take account of the very different magnitudes of energy flux encountered across the very wide range of planetary systems. In the approach presented here, we have shown not only the full values of the various terms in energy budgets in W m^{-2}, but also values in non-dimensional form with respect to the solar (or stellar) irradiance applicable at the respective planetary orbital distance. This allows an immediate comparison between the different ways in which different atmospheres scatter, absorb and transmit energy from and to space. It also suggests ways in which to classify different atmospheres, depending largely upon the density and opacity of each atmosphere to solar and thermal radiation.

Mars would appear to offer the simplest pattern of energy flow, at least under relatively dust-free conditions, in which the atmosphere appears to play a relatively minor role in absorbing and scattering both incoming and outgoing radiation. The energy balance at the surface is then largely determined by a direct exchange to space with only a modest greenhouse warming effect. It is important, however, to exercise some caution in interpreting this situation too simplistically. The low-dust case analyzed in section 3 utilized a model that essentially neglected the effects of clouds and assumed a dust distribution that was both tenuous and relatively uniform across the planet. This is only representative of Mars for part of the time. Moreover, it is now known that even fairly tenuous clouds of water ice can have a significant impact on the thermal structure and dynamics of the atmosphere (e.g. Wilson *et al.*, 2007, 2008; Madeleine *et al.*, 2012), even though their global impact on gross energy fluxes may remain relatively modest. This is partly due to the low density and

short radiative adjustment time-scale in the Martian atmosphere, though some of the effects entail some subtle nonlinear feedbacks. CO_2 also forms extensive clouds over the polar regions during winter (Pettengill and Ford, 2000; Hayne *et al.*, 2012). The radiative properties of CO_2 ice crystals are quite different from those of H_2O ice, in that the former are relatively reflective at both visible and infrared wavelengths, except in the vicinity of the 15 μm absorption band of CO_2 gas (Pierrehumbert, 2010). With particle sizes of order 10–100 μm, typical of well-developed clouds, CO_2 ice crystals are very efficient scatterers across almost the entire visible and infrared spectrum. This can allow dense CO_2 clouds to backscatter upwelling thermal radiation from the surface, effectively increasing the greenhouse warming of the surface and lower atmosphere (Hunt, 1980; Forget and Pierrehumbert, 1997; Pierrehumbert, 2010). Such effects have been suggested to be important for the early Martian climate (Forget and Pierrehumbert, 1997), though more recent work (e.g. Colaprete and Toon, 2003) seems to indicate that such clouds are rather less effective in warming the early Martian climate and are probably even less significant in the present Martian climate, apart perhaps from during polar winter.

During Martian planet-encircling dust storms, however, the effects of suspended dust modify the flow of radiative energy considerably, absorbing sunlight and scattering infrared emission from the surface. The net effect may be to induce an inverse greenhouse effect, which tends to cool the surface and temporarily overwhelm the greenhouse warming due to CO_2. The influence of dust is highly variable in time and very hard to predict, although some seasonal tendencies are reasonably clear. When a planet-encircling dust event does take place, however, it can alter the global energy balance for months at a time, so it needs to be taken into account in an evaluation of the Martian climate system.

At the other extreme, we encounter relatively dense and opaque atmospheres with Venus and Titan. Both are covered by fairly ubiquitous clouds, though composed of very different materials with differing scattering and absorption properties. Although this means that most of the incoming sunlight is processed in the upper, cloudy parts of the atmosphere, it leads to a very different partitioning of the incoming solar irradiance in the two cases. The clouds in Venus's atmosphere are highly reflective and scattering in the visible, to the extent that 76% of the incoming sunlight is scattered directly back into space without further interaction with the atmosphere. On Titan, however, only $\sim$ 20% of the incoming solar irradiance is scattered back to space, with around half being absorbed within the stratospheric clouds and hazes, leading to a pronounced anti-greenhouse effect in its stratosphere. In both cases, however, just a small fraction ($\sim$ 5–10%) of incoming sunlight reaches the surface of the planet. Together with the substantial opacity of the atmosphere in the infrared, this has the effect of creating a separate region in the deep atmosphere in both cases where the flow of thermal emission between atmosphere and surface is almost closed, feeding a significant positive greenhouse warming in the deep atmosphere. A small trickle of energy passes between the upper atmosphere and the surface due to the residue of solar radiation, some escape of upward thermal emission from the troposphere and some effects due to convective transfer of sensible heat. The latter appears to be significant in Titan's atmosphere, though the role of convection in Venus's deep atmosphere is currently quite uncertain. Indeed, much remains relatively unknown about the deep atmosphere of Venus, not least because of its inaccessibility to direct measurement, either *in situ* or via remote sensing.

In the context of these Solar System terrestrial planets, the energy budget of the Earth is seen to be a relatively complicated intermediate case, in which around half of the incoming sunlight reaches the surface, the rest being either scattered and reflected to space or absorbed within the atmosphere itself. In the infrared, the deep atmosphere has an almost closed exchange with the surface, though with significant exchanges due to convective transport of sensible and latent heat to balance the incoming sunlight. An important contribution on Earth also comes from the effects of evapotranspiration due to living plants and other organisms, something that is unique to the Earth. Some of the infrared absorbing greenhouse gases in the atmosphere (such as CH_4, N_2O and partly CO_2) also, of course, owe their presence to some extent to the action of living organisms, mediated by the ubiquitous effects of water in all three phases within the climate system. This ubiquitous presence of a large reservoir of a condensible species that can come into partial equilibrium with its vapour *and* also freeze to form ices is one of the unique aspects of the Earth's climate system, adding to its relative complexity compared with any other planet, with the possible exception of Titan (where an active analogue of the hydrological cycle is associated with hydrocarbons such as CH_4; see e.g. Lunine and Atreya, 2008). Thus, while some of the apparent complexity of the Earth's climate system compared with other known terrestrial planets may in part reflect our greater knowledge of the Earth, there may be good reasons why the Earth really is more complex than these other planets, associated with the unique presence of liquid water and the evolution of a living ecosystem.

Jupiter exhibits a few features in common with Venus and Titan in focusing the interactions between atmosphere and external irradiation into a layer near the top of the troposphere and lower stratosphere. There are, however, some important differences. For Jupiter, some 66% of incoming solar irradiance is absorbed directly by the atmosphere, with only around a third being reflected back to space. In addition, very little thermal radiation from deep levels actually makes it directly to space, with most of the radiation originating from the upper tropospheric levels. Another major difference from all of the terrestrial planets is the presence of a major heat source in the deep interior of Jupiter. This is likely to render much of the deep interior relatively strongly convective, with only the topmost regions (above around 1 bar) being dominated by radiative exchanges, although solar radiation penetrates to some extent down to several bar. This pattern is likely to be typical for all of the 'cold' gas and ice giant planets found in our Solar System, of whom all (except Uranus) are found to be significant net exporters of heat energy associated with long-term loss of primordial heat and slow gravitational collapse and differentiation.

The presence of a significant interior heat source emanating from within 'hot Jupiter' planets appears to be a relatively common occurrence although, as discussed in section 7.2, the precise mechanisms responsible for such a flux are not yet well understood. There also remain many uncertainties as to the mechanisms for how heat may be transported between daytime and night-time hemispheres. The magnitude of heat redistribution indicated in our analysis is somewhat smaller than that found in some studies of other hot Jupiter planets (Cowan *et al.*, 2007; Knutson *et al.*, 2007, 2009, 2012) and predicted by three-dimensional radiative–convective simulations (e.g. Showman *et al.*, 2009). Schwartz and Cowan (2015) find that a much larger fraction of the incoming heat is redistributed to the night side, but they use only broadband measurements to constrain the outgoing flux in the infrared, which may result in large amounts of flux escaping in relatively narrow, transparent wavelength regions being ignored. The evidence from these authors suggests only a 20–30% difference between day and night-side brightness temperatures, although Crossfield *et al.* (2012) and Majeau *et al.* (2012) suggest a rather larger difference, more like what we present in Figure 10. The gaps in the spectral coverage of the observations pose a major source of uncertainty, however, indicating a clear need for new observations, especially in the near-infrared, to constrain the energy exchanges more tightly.

Although 'hot Jupiter' class planets in close orbits around other stars have claimed a lot of attention as representing typical extrasolar planets, they are by no means the most common form of planet found around other stars. Recent work suggests that smaller planets with masses ranging from around 1–20

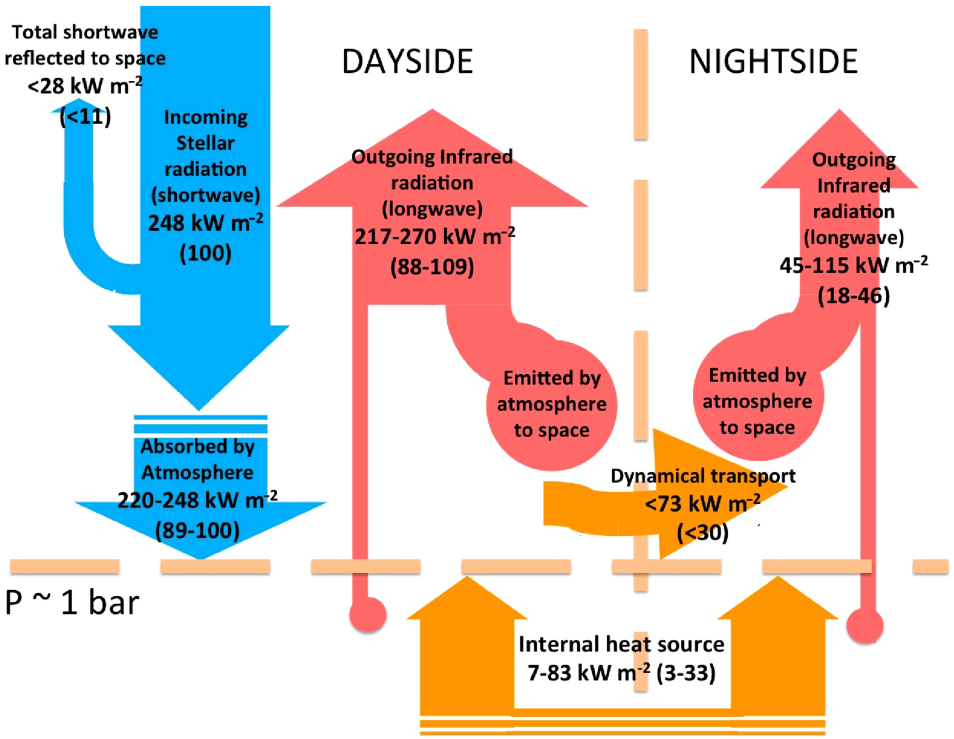

Figure 10. Schematic flow of energy within the strongly irradiated troposphere and stratosphere of the hot Jupiter exoplanet HD 189733b, as determined from a combination of astronomical measurements (Knutson *et al.*, 2012) and NEMESIS model calculations (Irwin *et al.*, 2008; Barstow *et al.*, 2014). Stellar radiative fluxes are shown on the left (in blue online) and infrared fluxes in the centre and on the right (salmon pink online); convective and dynamical heat fluxes are shown in the lower centre and upwelling from below (in orange online). The horizontal dashed line represents the approximate boundary in the atmosphere below which most of the stellar insolation does not penetrate, while the vertical dashed line separates the day from the night side.

Earth masses, around the same as Neptune at the high end, are much more common (e.g. Cassan *et al.*, 2012; Batalha *et al.*, 2013) and representative of more typical planets throughout the Galaxy. Such planets are likely to have substantial atmospheres and are already beginning to be found within the 'habitable zone' of their respective parent stars in a few cases. However, it is still quite uncertain as to whether they are likely then to possess very deep and extended, hydrogen-rich atmospheres (like Neptune itself) or shallow atmospheres overlying a solid, rocky planetary surface, like the Earth or Venus. The composition of such atmospheres is the subject of much current speculation, including the suggestion that some may be 'water worlds' with a 'steamy' atmosphere overlying deep oceans of liquid water. Recent observations have so far been unable to detect many spectral lines indicative of a particular composition. Indeed one of the more interesting interpretations of the relatively flat spectra obtained from transit measurements of some of these objects suggests that their atmospheres may be dense and cloudy (Moses, 2014). This would have major implications for their radiative energy budgets, although the clouds may be very different from anything we have encountered so far within the Solar System. However, it may be that the paradigms of Earth, Titan and Venus discussed here might be relevant to at least some of these planets. Given the significant uncertainties that remain in our calculations for HD 189733b, a planet for which we have good spectral coverage and phase curve information, we defer exploration of super-Earths and smaller worlds until the available data are of sufficient quality to provide some significant constraints.

Finally, it is important to note that determining the flow of energy through the climate system of a given planet is only one step along the road towards characterizing that climate system fully. A natural next step would be to use a knowledge of the fluxes of radiant and convective energy, together with the thermal structure of the atmosphere, to investigate other thermodynamic properties of the atmospheric heat engine, such as its thermodynamic efficiency (e.g. Ozawa *et al.*, 2003; Lucarini, 2009; Lucarini and Ragone, 2011; Schubert and Mitchell, 2013). Such calculations require knowledge of both the radiant fluxes and dynamical internal energy conversions, so can only really be computed from reasonably comprehensive 3D numerical simulations. Since these models are now reaching an appropriate level of sophistication for a number of other planets, this is likely to be a fruitful direction to explore in the future.

Acknowledgements

PLR, JB, PGJI and SRL acknowledge support from the UK Science and Technology Research Council and UK Space Agency during the course of this research under grant numbers ST/I001948/1, ST/J001597/1 and ST/I003096/1. PLR and SRL also acknowledge support from the European Space Agency. PLR is grateful to the Kavli Institute for Theoretical Physics at the University of California, Santa Barbara for their hospitality during the initial writing of this article. As a result, this research was supported in part by the US National Science Foundation under Grant No. NSF PHY11-25915. We are also grateful to three anonymous referees for their constructive comments on earlier versions of this article.

References

Abbot CG, Fowle FE. 1908. Radiation and terrestrial temperature. *Ann. Astrophys. Obs. Smithsonian Inst.* **2**: 125–224.

Atreya SK, Adams EY, Niemann HB, Demick-Montelara JE, Owen TC, Fulchignoni M, Ferri F, Wilson EH. 2006. Titan's methane cycle. *Planet. Space Sci.* **54**: 1177–1187, doi: 10.1016/j.pss.2006.05.028.

Avduevskiy VS, Marov MY, Kulikov YN, Shari VP, Gorbachevskiy AY, Uspenskiy GR, Cheremukhina ZP. 1983. Structure and parameters of the Venus atmosphere according to Venera Probe data. In *Venus*, Hunten DM, Colin L, Donahue TM, Moroz VI. (eds.): 280–298. University of Arizona Press: Tucson, AZ.

Barstow JK, Aigrain S, Irwin PGJ, Hackler T, Fletcher LN, Lee JM, Gibson NP. 2014. Clouds on the hot Jupiter HD 189733b: Constraints from the reflection spectrum. *Astrophys. J.* **786**: 154, doi: 10.1088/0004-637X/786/2/154.

Basu S, Richardson MI, Wilson RJ. 2004. Simulation of the Martian dust cycle with the GFDL Mars GCM. *J. Geophys. Res.* **109**: E11 006, doi: 10.1029/2004JE002243.

Batalha NM, Rowe JF, Bryson ST, Barclay T, Burke CJ, Caldwell DA, Christiansen JL, Mullally F, Thompson SE, Brown TM, Dupree AK, Fabrycky DC, Ford EB, Fortney JJ, Gilliland RL, Isaacson H, Latham DW, Marcy GW, Quinn SN, Ragozzine D, Shporer A, Borucki WJ, Ciardi DR, Gautier III TN, Haas MR, Jenkins JM, Koch DG, Lissauer JJ, Rapin W, Basri GS, Boss AP, Buchhave LA, Carter JA, Charbonneau D, Christensen-Dalsgaard J, Clarke BD, Cochran WD, Brice-Olivier D, Desert J-M, Devore E, Doyle LR, Esquerdo GA, Everett M, Fressin F, Geary JC, Girouard FR, Gould A, Hall JR, Holman MJ, Howard AW, Howell SB, Ibrahim KA, Kinemuchi K, Kjeldsen H, Klaus TC, Li J, Lucas PW, Meibom S, Morris RL, Prsa A, Quintana E, Sanderfer DT, Sasselov D, Seader SE, Smith JC, Steffen JH, Still M, Stumpe MC, Tarter JC, Tenenbaum P, Torres G, Twicken JD, Uddin K, Van Cleve J, Walkowicz L, Welsh WF. 2013. Planetary candidates observed by Kepler. III. Analysis of the first 16 months of data. *Astrophys. J. Suppl. Ser.* **204**: 24.

Bouchy F, Udry S, Mayor M, Moutou C, Pont F, Iribarne N, da Silva R, Ilovaisky S, Queloz D, Santos NC, Ségransan D, Zucker S. 2005. ELODIE metallicity-biased search for transiting hot Jupiters. II. A very hot Jupiter transiting the bright K star HD 189733. *Astron. Astrophys.* **444**: L15–L19.

Cassan A, Kubas D, Beaulieu JP, Dominik M, Horne K, Greenhill J, Wambsganss J, Menzies J, Williams A, Jørgensen UG, Udalski A, Bennett DP, Albrow MD, Batista V, Brillant S, Caldwell JAR, Cole A, Coutures Ch, Cook KH, Dieters S, Dominis Prester D, Donatowicz J, Fouqué P, Hill K, Kains N, Kane S, Marquette JB, Martin R, Pollard KR, Sahu KC, Vinter C, Warren D, Watson B, Zub M, Sumi T, Szymanski MK, Kubiak M, Poleski R, Soszynski I, Ulaczyk K, Pietrzynski G, Wyrzykowski L. 2012. One or more bound planets per Milky Way star from microlensing observations. *Nature* **481**: 167–169.

Charnay B, Lebonnois S. 2012. Two boundary layers in Titan's lower troposphere inferred from a climate model. *Nat. Geosci.* **5**: 106–109, doi: 10.1038/ngeo1374.

Christensen P, Bandfield J, Hamilton V, Ruff S, Kieffer H, Titus T, Malin M, Morris R, Lane M, Clark R, Jakosky B, Mellon M, Pearl J, Conrath B, Smith M, Clancy R, Kuzmin R, Roush T, Mehall G, Gorelick N, Bender K, Murray K, Dason S, Greene E, Silverman S, Greenfield M. 2001. Mars Global Surveyor Thermal Emission Spectrometer experiment: Investigation description and surface science results. *J. Geophys. Res.* **106**: 23 823–23 871, doi: 10.1029/2000JE001370.

Colaprete A, Toon AB. 2003. Carbon dioxide clouds in an early dense Martian atmosphere. *J. Geophys. Res.* **108**: 5025, doi: 10.1029/2002JE001967.

Cowan N, Agol E, Charbonneau D. 2007. Hot nights on extrasolar planets: Mid-infrared phase variations of hot Jupiters. *Mon. Not. R. Astron. Soc.* **379**: 641–646.

Crisp D. 1985. Radiative forcing of the Venus mesosphere. II. Thermal fluxes, cooling rates, and radiative equilibrium temperatures. *Icarus* **77**: 391–413.

Crossfield IJ, Knutson H, Fortney J, Showman AP, Cowan NB, Deming D. 2012. Spitzer/MIPS 24 μm observations of HD 109458b: Three eclipses, two and a half transits and a phase curve corrupted by instrumental sensitivity variations. *Astrophys. J.* **752**: 81.

Dines WH. 1917. The heat balance of the atmosphere. *Q. J. R. Meteorol. Soc.* **43**: 151–158.

Evans TM, Pont F, Sing DK, Aigrain S, Barstow JK, Désert JM, Gibson N, Heng K, Knutson HA, Lecavelier des Etangs A. 2013. The deep blue color of HD 189733b: Albedo measurements with Hubble space telescope/space telescope imaging spectrograph at visible wavelengths. *Astrophys. J. Lett.* **772**: L16, doi: 10.1088/2041-8205/772/2/L16.

Forget F, Pierrehumbert RT. 1997. Warming early Mars with carbon dioxide clouds that scatter infrared radiation. *Science* **278**: 1273–1276.

Forget F, Hourdin F, Fournier R, Hourdin C, Talagrand O, Collins M, Lewis SR, Read PL, Huot JP. 1999. Improved general circulation models of the Martian atmosphere from the surface to above 80 km. *J. Geophys. Res.* **104**: 24 155–24 176, doi: 10.1029/1999JE001025.

Forget F, Gonzalez-Galindo F, Lebonnois S, Bertaux JL, Montmessin F, Quémerais E, Reberac A, Dimarellis E, Valverde MAL. 2009. The density and temperatures of the upper Martian atmosphere measured by stellar occultations with Mars Express SPICAM. *J. Geophys. Res.* **114**: E01 004, doi: 10.1029/2008JE003086.

Fortney JF, Baraffe I, Militzer B. 2010. Giant planet interior structure and thermal evolution. In *Exoplanets*, Seager S. (ed.): 397. University of Arizona Press: Tucson, AZ.

Fulchignoni M, Ferri F, Angrilli F, Ball AJ, Bar-Nun A, Barucci MA, Bettanini C, Bianchini G, Borucki W, Colombatti G, Coradini M, Coustenis A, Debei S, Falkner P, Fanti G, Flamini E, Gaborit V, Grard R, Hamelin M, Harri AM, Hathi B, Jernej I, Leese MR, Lehto A, Lion Stoppato PF, López-Moreno JJ, Mäkinen T, McDonnell JAM, McKay CP, Molina-Cuberos G, Neubauer FM, Pirronello V, Rodrigo R, Saggin B, Schwingenschuh K, Seiff A, Simões F, Svedhem H, Tokano T, Towner MC, Trautner R, Withers P, Zarnecki JC. 2005. In situ measurements of the physical characteristics of Titan's environment. *Nature* **438**: 785–791, doi: 10.1038/nature04314.

Greybush SJ, Wilson RJ, Hoffman RN, Hoffman MJ, Miyoshi T, Ide K, McConnochie T, Kalnay E. 2012. Ensemble Kalman filter data assimilation of Thermal Emission Spectrometer temperature retrievals into a Mars GCM. *J. Geophys. Res.* **117**: E11 008, doi: 10.1029/2012JE004097.

Guillot T, Stevenson DJ, Hubbard WB, Saumon D. 2004. The interior of Jupiter. In *Jupiter: The Planet, Satellites and Magnetosphere*, Bagenal F, Dowling TE, McKinnon WB. (eds.): 35–57. Cambridge University Press: Cambridge, UK.

Haberle RM, Pollack JB, Barnes JR, Zurek RW, Leovy CB, Murphy JR, Lee H, Schaeffer J. 1993. Mars atmospheric dynamics as simulated by the NASA/Ames general circulation model, 1. The zonal-mean circulation. *J. Geophys. Res.* **98**: 3093–3123, doi: 10.1029/92JE02946.

Hanel RA, Conrath BJ, Herath LW, Kunde VG, Pirraglia JA. 1981. Albedo, internal heat, and energy balance of Jupiter: Preliminary results of the Voyager infrared investigation. *J. Geophys. Res.* **86**: 8705–8712, doi: 10.1029/JA086iA10p08705.

Hansen J, Sato M, Kharecha P, von Schuckmann K. 2011. Earth's energy imbalance and implications. *Atmos. Chem. Phys.* **11**: 13421–13449.

Harrison EF, Minnis P, Barkstrom BR, Ramanathan V, Cess RD, Gibson GG. 1990. Seasonal variation of cloud radiative forcing derived from the Earth Radiation Budget Experiments. *J. Geophys. Res.* **95**: 18687–18703, doi: 10.1029/JD095iD11p18687.

Hayne PO, Paige DA, Schofield JT, Kass DM, Kleinböhl A, Heavens NG, McCleese DJ. 2012. Carbon dioxide snow clouds on Mars: South polar winter observations by the Mars Climate Sounder. *J. Geophys. Res.* **117**: E08 014, doi: 10.1029/2011JE004040.

Helling C, Woitke P, Thi WF. 2008. Dust in brown dwarfs and extrasolar planets. I. Chemical composition and spectral appearance of quasi-static cloud layers. *Astron. Astrophys.* **485**: 547–560, doi: 10.1051/0004-6361:20078220.

Hess SL, Ryan JA, Tillman JE, Henry RM, Leovy CB. 1980. The annual cycle of pressure on Mars measured by Viking Landers 1 and 2. *Geophys. Res. Lett.* **7**: 197–200, doi: 10.1029/GL007i003p00197.

Hourdin F, Talagrand O, Sadourny R, Courtin R, Gautier D, McKay CP. 1995. Numerical simulation of the general circulation of the atmosphere of Titan. *Icarus* **117**: 358–374.

Hubbard WN. 1968. Thermal structure of Jupiter. *Astrophys. J.* **152**: 745–754.

Hubbard WN. 1977. The Jovian surface condition and cooling rate. *Icarus* **30**: 305–310.

Hunt GE. 1980. On the infrared radiative properties of CO ice clouds: Application to Mars. *Geophys. Res. Lett.* **7**: 481–484, doi: 10.1029/GL007i007p00481.

IPCC. 2013. Working group I Contribution to the Intergovernmental Panel on Climate Change Fifth Assessment Report: The Physical Science Basis. IPCC Fifth Assessment Report – Climate Change 2013. World Meteorological Organization: Geneva, Switzerland.

Irwin PGJ, Parrish PD, Fouchet T, Calcutt SB, Taylor FW, Simon-Miller AA, Nixon CA. 2005. Retrievals of Jovian tropospheric phosphine from Cassini/CIRS. *Icarus* **172**: 37–49.

Irwin PGJ, Teanby NA, de Kok R, Fletcher LN, Howett CJA, Tsang CCC, Wilson CF, Calcutt SB, Nixon CA, Parrish PD. 2008. The NEMESIS planetary atmosphere radiative transfer and retrieval tool. *J. Quant. Spectrosc. Radiat. Transfer* **109**: 1136–1150.

Kiehl JT, Trenberth KE. 1997. Earth's annual global mean energy budget. *Bull. Am. Meteorol. Soc.* **78**: 197–208.

Kim D, Ramanathan V. 2012. Improved estimates and understanding of global albedo and atmospheric solar absorption. *Geophys. Res. Lett.* **39**: D02203, doi: 10.1029/2012GL053757.

Knutson HA, Charbonneau D, Allen LE, Fortney JJ, Agol E, Cowan NB, Showman AP, Cooper CS, Megeath ST. 2007. A map of the day–night contrast of the extrasolar planet HD 189733b. *Nature* **447**: 183–186.

Knutson HA, Charbonneau D, Cowan NB, Fortney JJ, Showman AP, Agol E, Henry GW, Everett ME, Allen LE. 2009. Multiwavelength constraints on the day–night circulation patterns of HD 189733b. *Astrophys. J.* **690**: 822.

Knutson HA, Lewis N, Fortney JJ, Burrows A, Showman AP, Cowan NB, Agol E, Aigrain S, Charbonneau D, Deming D, Désert JM, Henry GW, Langton J, Laughlin G. 2012. 3.6 and 4.5 μm phase curves and evidence for non-equilibrium chemistry in the atmosphere of extrasolar planet HD 189733b. *Astrophys. J.* **754**: 22.

Kopp G, Lean JL. 2011. A new, lower value of total solar irradiance: Evidence and climate significance. *Geophys. Res. Lett.* **38**: L01 706, doi: 10.1029/2010GL045777.

Lebonnois S, Covey C, Grossman A, Parish H, Schubert G, Walterscheid R, Lauritzen P, Jablonowski C. 2012. Angular momentum budget in General Circulation Models of superrotating atmospheres: A critical diagnostic. *J. Geophys. Res.* **117**: E12004, doi: 10.1029/2012JE004223.

Lebonnois S, Eymet V, Lee C, Vatant dOllone J. 2015. Analysis of the radiative budget of the Venusian atmosphere based on infrared Net Exchange Rate formalism. *J. Geophys. Res.* **120**: 1186–1200, doi: 10.1002/2015JE004794.

Lee C, Richardson MI. 2011. A discrete ordinate, multiple scattering, radiative transfer model of the Venus atmosphere from 0.1 to 260 μm. *J. Atmos. Sci.* **68**: 1323–1339.

Lewis SR, Collins M, Read PL, Forget F, Hourdin F, Fournier R, Hourdin C, Talagrand O, Huot JP. 1999. A climate database for Mars. *J. Geophys. Res.* **104**: 24 177–24 194, doi: 10.1029/1999JE001024.

Lewis SR, Read PL, Conrath BJ, Pearl JC, Smith MD. 2007. Assimilation of Thermal Emission Spectrometer atmospheric data during the Mars Global Surveyor aerobraking period. *Icarus* **192**: 327–347.

Li L, Nixon CA, Achterberg RK, Smith MA, Gorius NJP, Jiang X, Conrath BJ, Gierasch PJ, Simon-Miller AA, Flasar FM, Baines KH, Ingersoll AP, West RA, Vasavada AR, Ewald SP. 2011. The global energy balance of Titan. *Geophys. Res. Lett.* **38**: L23 201, doi: 10.1029/2011GL050053.

Li L, Baines KH, Smith MA, West RA, Pérez-Hoyos S, Trammell HJ, Simon-Miller AA, Conrath BJ, Gierasch PJ, Orton GS, Nixon CA, Filacchione G, Fry PM, Momary TW. 2012. Emitted power of Jupiter based on Cassini CIRS and VIMS observations. *J. Geophys. Res.* **117**: E11 002, doi: 10.1029/2012JE004191.

Limaye SS, Rengel M. 2013. Atmospheric circulation and dynamics. In *Towards Understanding the Climate of Venus: Applications of Terrestrial Models to Our Sister Planet*, Bengtsson L, Bonnet RM, Grinspoon D, Koumoutsaris S, Lebonnois S, Titov D. (eds.): 55–70. Springer: New York, NY.

Loeb NG, Lyman JM, Johnson GC, Allan RP, Doelling DR, Wong T, Soden BJ, Stephens GL. 2012. Observed changes in top-of-the-atmosphere radiation and upper-ocean heating consistent within uncertainty. *Nat. Geosci.* **5**: 110–113, doi: 10.1038/ngeo1375.

Lorenz EN. 1955. Available potential energy and the maintenance of the general circulation. *Tellus* **7**: 157–167.

Lorenz EN. 1967. *The Nature and Theory of the General Circulation of the Atmosphere*. No. 218, T. P. 115, WMO: Geneva, Switzerlan.

Low FJ. 1966. Observations of Venus, Jupiter and Saturn at $\lambda 20\mu$. *Astron. J.* **71**: 391.

Lucarini V. 2009. Thermodynamic efficiency and entropy production in the climate system. *Phys. Rev. E* **80**: 021 118.

Lucarini V, Ragone F. 2011. Energetics of climate models: Net energy balance and meridional enthalpy transport. *Rev. Geophys.* **49**: RG1001.

Lunine JI, Atreya SK. 2008. The methane cycle on Titan. *Nat. Geosci.* **1**: 159–164.

McCleese DJ, Heavens NG, Schofield JT, Abdou WA, Bandfield JL, Calcutt SB, Irwin PGJ, Kass DM, Kleinböhl A, Lewis SR, Paige DA, Read PL, Richardson MI, Shirley JH, Taylor FW, Teanby N, Zurek RW. 2010. Structure and dynamics of the Martian lower and middle atmosphere as observed by the Mars Climate Sounder: Seasonal variations in zonal mean temperature, dust, and water ice aerosols. *J. Geophys. Res.* **115**: E12 016, doi: 10.1029/2010JE003677.

Madeleine JB, Forget F, Millour E, Navarro T, Spiga A. 2012. The influence of radiatively active water ice clouds on the Martian climate. *Geophys. Res. Lett.* **39**: L23 202, doi: 10.1029/2012GL053564.

McKay CP, Pollack JB, Courtin R. 1991. The greenhouse and antigreenhouse effects on Titan. *Science* **253**: 1118–1121.

Majeau C, Agol E, Cowan NB. 2012. A two-dimensional infrared map of the extrasolar planet HD 189733b. *Astrophys. J. Lett.* **747**: L20, doi: 10.1088/2041-8205/747/2/L20.

Mendonça JM. 2013. 'Studies of Venus using a comprehensive general circulation model', PhD thesis. University of Oxford: Oxford, UK.

Mendonça JM, Read PL, Wilson CF, Lee C. 2015. New fast and flexible radiative transfer method for Venus general circulation models. *Planet. Space Sci.* **105**: 80–93.

Mitchell JL. 2012. Titan's transport-driven methane cycle. *Astrophys. J. Lett.* **756**: L26.

Montabone L, Lewis SR, Read PL, Hinson DP. 2006. Validation of Martian meteorological data assimilation for MGS/TES using radio occultation measurements. *Icarus* **185**: 113–132.

Montabone L, Marsh K, Lewis SR, Read PL, Smith MD, Holmes J, Spiga A, Lowe D, Pamment A. 2014. The Mars analysis correction data sssimilation (MACDA) Dataset V1.0. *Geosci. Data J.* **1**: 129–139, doi: 10.1002/gdj3.13.

Montabone L, Forget F, Millour E, Wilson RJ, Lewis SR, Cantor B, Kass D, Kleinböhl A, Lemmon MT, Smith M, Wolff MJ. 2015. Eight-year climatology of dust optical depth on Mars. *Icarus* **251**: 65–95, doi: 10.1016/j.icarus.2014.12.034.

Morley CV, Fortney JJ, Marley MS, Visscher C, Saumon D, Leggett SK. 2012. Neglected clouds in T and Y dwarf atmospheres. *Astrophys. J.* **756**: 172, doi: 10.1088/0004-637X/756/2/172.

Moses JL. 2014. Cloudy with a chance of dustballs. *Nature* **505**: 31–32.

Müller-Wodarg I, Griffith CA, Lellouch E, Cravens TE. (eds.) 2014. *Titan*. Cambridge University Press: Cambridge, UK.

Newman CE, Lewis SR, Read PL, Forget F. 2002. Modeling the Martian dust cycle, 1. Representations of dust transport processes. *J. Geophys. Res.* **107**(E12): 5123, doi: 10.1029/2002JE001 910.

Ozawa H, Ohmura A, Lorenz RD, Pujol T. 2003. The second law of thermodynamics and the global climate system: A review of the Maximum Entropy Production principle. *Rev. Geophys.* **41**: 4.

Pearl JC, Conrath BJ, Hanel RA, Pirraglia JA, Coustenis A. 1990. The albedo, effective temperature, and energy balance of Uranus, as determined from Voyager IRIS data. *Icarus* **84**: 12–28.

Peixoto JP, Oort AH. 1992. *Physics of Climate*. American Institute of Physics: New York, NY.

Pettengill GH, Ford PG. 2000. Winter clouds over the north Martian polar cap. *Geophys. Res. Lett.* **27**: 609–612, doi: 10.1029/1999GL010896.

Pierrehumbert RT. 2010. *Principles of Planetary Climate*. Cambridge University Press: Cambridge, UK.

Plass GN, Kattawar GW, Catchings FE. 1973. Matrix operator theory of radiative transfer. 1: Rayleigh scattering. *Appl. Opt.* **12**: 314–329.

Pollack JB. 1979. Climatic change on the terrestrial planets. *Icarus* **37**: 479–553.

Putzig NE, Mellon MT, Kretke KA, Arvidson RE. 2005. Global thermal inertia and surface properties of Mars from the MGS mapping mission. *Icarus* **173**: 325–341.

Rannou P, Hourdin F, McKay CP, Luz DA. 2004. A coupled dynamics–microphysics model of Titan's atmosphere. *Icarus* **170**: 443–462.

Rauscher E, Menou K. 2013. Three-dimensional atmospheric circulation models of HD 189733b and HD 209458b with consistent magnetic drag and ohmic dissipation. *Astrophys. J.* **764**: 103.

Read PL. 2013. The dynamics and circulation of Venus' atmosphere. In *Towards Understanding the Climate of Venus: Applications of Terrestrial Models to Our Sister Planet*, Bengtsson L, Bonnet RM, Grinspoon D, Koumoutsaris S, Lebonnois S, Titov D. (eds.): 73–110. Springer: New York, NY.

Read PL, Lewis SR. 2004. *The Martian Climate Revisited*. Springer-Praxis: Berlin & Heidelberg.

Revercomb HE, Sromovsky LA, Suomi VE, Boese RW. 1985. Net thermal radiation in the atmosphere of Venus. *Icarus* **61**: 521–538.

Robinson TD, Catling DC. 2012. An analytic radiative–convective model for planetary atmospheres. *Astrophys. J.* **757**: 104.

Robinson TD, Catling DC. 2014. Common 0.1 bar tropopause in thick atmospheres set by pressure-dependent infrared transparency. *Nat. Geosci.* **7**: 12–15.

Rodriguez S, Le Mouélic S, Rannou P, Sotin C, Brown RH, Barnes JW, Griffith CA, Burgalat J, Baines KH, Buratti BJ, Clark RN, Nicholson PD. 2011. Titan's cloud seasonal activity from winter to spring with Cassini/VIMS. *Icarus* **216**: 89–110, doi: 10.1016/j.icarus.2011.07.031.

Sagan C. 1969. Gray and non gray planetary atmospheres: Structure, convective instability and greenhouse effect. *Icarus* **10**: 290–300.

Schneider J, Dedieu C, Le Sidaner P, Savalle R, Zolotukhin I. 2011. Defining and cataloging exoplanets: The exoplanet.eu database. *Astron. Astrophys.* **532**: doi: 10.1051/0004-6361/201116713.

Schubert G, Mitchell JL. 2013. Planetary atmospheres as heat engines. In *Comparative Climatology of Terrestrial Planets*, Mackwell SJ, Simon-Miller AA, Harder JW, Bullock MA. (eds.): 181–191. University of Arizona Press: Tucson, AZ.

Schwartz JC, Cowan NB. 2015. Balancing the energy budget of short-period giant planets: Evidence for reflective clouds and optical absorbers. *Mon. Not. R. Astr. Soc.* **449**(4): 4192–4203, doi: 10.1093/mnras/stv470.

Seiff A, Kirk DB, Young RE, Blanchard RC, Findlay JT, Kelly GM, Sommer SC. 1980. Measurements of thermal structure and thermal contrasts in the atmosphere of Venus and related dynamical observations – results from the four Pioneer Venus probes. *J. Geophys. Res.* **85**: 7903–7933, doi: 10.1029/JA085iA13p07903.

Showman AP, Fortney JJ, Lian Y, Marley MS, Freedman RS, Knutson HA, Charbonneau D. 2009. Atmospheric circulation of hot Jupiters: Coupled radiative–dynamical general circulation model simulations of HD 189733b and HD 209458b. *Astrophys. J.* **699**: 564–584, doi: 10.1088/0004-637X/699/1/564.

Showman AP, Cho J, Menou K. 2010. Atmospheric circulation of extrasolar planets. In *Exoplanets*, Seager S. (ed.): 471–516. University of Arizona Press: Tucson, AZ.

Smith MD, Bandfield JL, Christensen PR, Richardson MI. 2003. Thermal Emission Imaging System (THEMIS) infrared observations of atmospheric dust and water ice cloud optical depth. *J. Geophys. Res.* **108**: 5115, doi: 10.1029/2003JE002115.

Sromovsky LA, Collard AD, Fry PM, Orton GS, Lemmon MT, Tomasko MG, Freedman RS. 1998. Galileo probe measurements of thermal and solar radiation fluxes in the Jovian atmosphere. *J. Geophys. Res.* **103**: 22 929–22 977, doi: 10.1029/98JE01048.

Stephens GL, Li J, Wild M, Clayson CA, Loeb N, Kato S, L'Ecuyer T, Stackhouse PW, Jr, Lebsock M, Andrews T. 2012. An update on Earth's energy balance in light of the latest global observations. *Nat. Geosci.* **5**: 691–696.

Stofan ER, Elachi C, Lunine JI, Lorenz RD, Stiles B, Mitchell KL, Ostro S, Soderblom L, Wood C, Zebker H, Wall S, Janssen M, Kirk R, Lopes R, Paganelli F, Radebaugh J, Wye L, Anderson Y, Allison M, Boehmer R, Callahan P, Encrenaz P, Flamini E, Francescetti G, Gim Y, Hamilton G, Hensley S, Johnson WTK, Kelleher K, Muhleman D, Paillou P, Picardi G, Posa F, Roth L, Seu R, Shaffer S, Vetrella S, West R. 2007. The lakes of Titan. *Nature* **445**: 61–64.

Taylor FW. 2010. *Planetary Atmospheres*. Oxford University Press: Oxford, UK.

Titov DV, Piccioni G, Drossart P, Markiewicz WJ. 2013. Radiative energy balance in the Venus atmosphere. In *Towards Understanding the Climate of Venus: Applications of Terrestrial Models to Our Sister Planet*, Bengtsson L, Bonnet RM, Grinspoon D, Koumoutsaris S, Lebonnois S, Titov D. (eds.): 23–53. Springer: New York, NY.

Tomasko MG, Doose LR, Smith PH, Odell AP. 1980. Measurements of the flux of sunlight in the atmosphere of Venus. *J. Geophys. Res.* **85**: 8167–8186, doi: 10.1029/JA085iA13p08167.

Tomasko MG, Bézard B, Doose L, Engel S, Karkoschka E, Vinatier S. 2008. Heat balance in Titan's atmosphere. *Planet. Space Sci.* **56**: 648–659, doi: 10.1016/j.pss.2007.10.012.

Trenberth KE, Fasullo JT. 2012. Tracking Earth's energy: From El Niño to global warming. *Surv. Geophys.* **33**: 413–426.

Trenberth KE, Fasullo JT, Kiehl J. 2009. Earth's global energy budget. *Bull. Am. Meteorol. Soc.* **90**: 311–323.

Turtle EP, Del Genio AD, Barbara JM, Perry JE, Schaller EL, McEwen AS, West RA, Ray TL. 2011. Seasonal changes in Titan's meteorology. *Geophys. Res. Lett.* **38**: L03203, doi: 10.1029/2010GL046266.

Vonder Haar TH, Suomi V. 1971. Measurements of the Earth's radiation budget from satellites during a 5 year period. I. Extended time and space means. *J. Atmos. Sci.* **28**: 305–314.

West RA, Baines KH, Friedson AJ, Banfield D, Ragent B, Taylor FW. 2004. Jovian clouds and haze. In *Jupiter: The Planet, Satellites and Magnetosphere*, Bagenal F, Dowling TE, McKinnon WB. (eds.): 79–104. Cambridge University Press: Cambridge, UK.

Wielicki BA, Barkstrom BR, Harrison EF, Lee RB, Smith G, Cooper JE. 1996. Clouds and the Earth's Radiant Energy System (CERES): An Earth observing system experiment. *Bull. Am. Meteorol. Soc.* **77**: 853–868.

Wild M, Folini D, Schär C, Loeb N, Dutton EG, König-Langlo G. 2013. The global energy balance from a surface perspective. *Clim. Dyn.* **40**: 3107–3134.

Williams KE, McKay CP, Persson F. 2012. The surface energy balance at the Huygens landing site and the moist surface conditions on Titan. *Planet. Space Sci.* **60**: 376–385.

Wilson RJ, Neumann GA, Smith MD. 2007. Diurnal variation and radiative influence of Martian water ice clouds. *Geophys. Res. Lett.* **34**: L02 710, doi: 10.1029/2006GL027976.

Wilson RJ, Lewis SR, Montabone L, Smith MD. 2008. Influence of water ice clouds on Martian tropical atmospheric temperatures. *Geophys. Res. Lett.* **35**: L07 202, doi: 10.1029/2007GL032405.

Wolff MJ, Smith MD, Clancy RT, Spanovich N, Whitney BA, Lemmon MT, Bandfield JL, Banfield D, Ghosh A, Landis G, Christensen PR, Bell JF III, Squyres SW. 2006. Constraints on dust aerosols from the Mars Exploration Rovers using MGS overflights and Mini-TES. *J. Geophys. Res.* **111**: E12S17, doi: 10.1029/2006JE002786.

Wolkenberg P, Grassi D, Formisano V, Rinaldi G, D'Amore M, Smith M. 2009. Simultaneous observations of the Martian atmosphere by Planetary Fourier Spectrometer on Mars Express and Miniature Thermal Emission Spectrometer on Mars Exploration Rover. *J. Geophys. Res.* **114**: E04 012, doi: 10.1029/2008JE003216.